Effect of the addition of iron oxide on the microstructure of ye'elimite

F.Z. Abir, M. Mesnaoui, Y. Abouliatim, L. Nibou, Tariq Labbilta, Y. El Hafiane, A. Smith

Version of Record: https://www.sciencedirect.com/science/article/pii/S000888462100274X
Manuscript_2e94278ee2378ed618851734efaf0755

Effect of the addition of iron oxide on the microstructure of ye'elimite

F. Z. Abir[1,2,3], M. Mesnaoui[2,4], Y. Abouliatim[3], L. Nibou[5], Tariq Labbilta[2], Y. El Hafiane[1], A. Smith[1]

1 : Institute of Research on Ceramics (IRCER), UMR 7315 CNRS – Université de Limoges – Centre Européen de la Céramique, 12 rue Atlantis, 87068 Limoges cedex, France

2 : Laboratoire de Sciences des Matériaux et Optimisation des Procédés FSSM – Université Cadi Ayyad, Marrakech 40000, Morocco

3 : Laboratoire Matériaux Procédés Environnement Qualité (LMPEQ) – Université Cadi Ayyad, École Nationale des Sciences Appliquées de Safi, Morocco

4 : Center for Soil and Fertilizer Research in Africa (CESFRA) – Mohammed VI Polytechnic University, Benguerir, Morocco

5 : Laboratoire Ingénierie des Systèmes & Applications (LISA) – Université Cadi Ayyad, École Nationale des Sciences Appliquées de Marrakech, BP 575 Avenue Abdelkrim Khattabi, Guéliz, Marrakech, Morocco

Abstract

This article is devoted to the description of the microstructure of ye'elimite, calcium aluminates and ferritic phase when iron oxide is present and when the synthesis is carried out at 1300 °C for 3h. The incorporation of iron in ye'elimite structure (general formula: $Ca_4Al_{(6-2x)}Fe_{2x}SO_{16}$ with x = 0.00 to 1.13) is complete when x < 0.12. Beyond this composition, the ferritic phase $(CaO)_2(Al_2O_3,Fe_2O_3)$ appears as a minor phase which can develop two forms: needle-like morphology and melt morphology. The presence of iron favors the formation of an iron-rich liquid phase which leads to the growth of ye'elimite grains by material diffusion mechanisms and increases the conversion rate of alumina and calcium aluminates in ye'elimite phase. Also a clear distinction between calcium aluminate and ye'elimite grains is presented.

Keywords: Ye'elimite, Microstructure, Ferritic phase, EDS mapping, Thermal Treatment.

Effect of the addition of iron oxide on the microstructure of ye'elimite

1. Introduction

Cement is the most widely used constituent in the construction industry as a binder material in concrete. The cement industry continues to look for less polluting and alternative binders to Portland clinkers. Calcium Sulfoaluminate Cements (CSA) represent one alternative. Since the 1970's, research on the Calcium Sulfoaluminate Cements (CSA) concerns various characteristics of these cements, such as shrinkage compensation, their high early strengths [1], or its use for rapid-setting applications. These binders present other advantages: reduction of CO_2 emissions, energy saving [2] when compared to Ordinary Portland Cements (OPC), because the sintering temperature of CSA cements is in range of 1250 to 1350 °C, which means 100 up to 200 °C lower compared to OPC and lower grinding energy.

The raw materials used for CSA synthesis, namely calcium carbonate, gypsum and alumina, can contain minor elements which can influence the mineralogy and hydraulic reactivity of the clinker phases. One of these elements is iron. It comes from alumina source such as bauxite and red mud which can present high proportions of iron [3]. The studies presented in the literature about the effect of iron focus (i) on the preparation of CSA compositions, (ii) on the crystallographic description of the CSA phases and (iii) on the hydration behaviour. The main information related to two items (i) and (ii) are given in the next paragraphs. Since the present work does not deal with hydration, bibliographic data related to this topic will not be presented.

1.1 Preparation of CSA compositions containing iron

Ye'elimite $C_4A_3\overline{S}$* represents the main phase of CSA clinker [4–6]. During the production of CSA cements, it was reported that iron oxide promotes the formation of ye'elimite $C_4A_3\overline{S}$ [3,7,8]. In the literature, some papers report the effect of Fe_2O_3 on the formation of ye'elimite [3,9–16], using different preparation protocols. Table 1 summarizes the synthesis conditions of ye'elimite described in the literature. The raw materials are usually $CaCO_3$, Al_2O_3, $CaSO_4.2H_2O$ and Fe_2O_3. Samples containing different amounts of iron were studied and sintered at temperatures between 1250 °C and 1350 °C. In some cases, the description of the preparation protocol in incomplete; the amount of raw materials, the sintering cycle (temperature, time, ramps) is sometimes missing. Moreover, each preparation method gives different results with respect to the formed secondary phases, their crystal structure and the maximum level of inserted iron. Secondly, depending on the published data, the percentages of iron are expressed in various units: weight percentage of Fe in $C_4A_3\overline{S}$, number of moles of Fe_2O_3 in the general formula $3CaCO_3 – (3 - x)Al_2O_3 – xFe_2O_3 – CaSO_4.2H_2O$, weight percentage of Fe_2O_3 in the mixture of $CaCO_3$, Al_2O_3, Fe_2O_3 and $CaSO_4.2H_2O$, weight percentage of Fe_2O_3 in the mixture of CaO, Al_2O_3, Fe_2O_3 and SO_3. In order to compare the different literature data, we have calculated the molar content, x, of Al_2O_3 substituted by Fe_2O_3 in the general formula ($Ca_4Al_{(6-2x)}Fe_{2x}SO_{16}$ or $C_4A_{3-x}F_x\overline{S}$). The values are presented in Table 1.

* Cement notation: C = CaO, A = Al_2O_3, $\overline{S}$ = SO_3, $\overline{C}$ = CO_2, H = H_2O, F = Fe_2O_3, M = MgO

1.2 Nature and crystallographic structure of phases in CSA containing iron

Some authors have shown that Fe^{3+} ions can replace Al^{3+} ions in the ye'elimite structure [3,12]. Various research groups investigated the iron content in $C_4A_{3-x}F_x\overline{S}$ solid solutions, but the reported experimental values are different. J. Strigac et al. [13] presented a study on sulfoaluminate belite cements where they reported the existence of a ye'elimite phase for x ~ 0.08. Another study [9] examined the substitution of aluminum by iron in the structure of ye'elimite of general formula $C_4A_{3-x}F_x\overline{S}$, where $0 < x < 0.8$. The maximum substitution level was defined at (x ~ 0.27), which is in agreement with the results of [14] and [16] who studied the coexistence of ye'elimite and ferritic phases at 1325 °C. The existence of a compound formed with 10 wt% Fe_2O_3 (x ~ 0.3) [15] has also been claimed. D. Chen et al. [11] reported that the condition for Fe_2O_3 to reach the maximum solid solution in ye'elimite is about 22.6 wt% Fe_2O_3 in the preparation process, which corresponds to (x = 1.2). In another investigation [3], the reported maximum iron concentration in ye'elimite is 21.5 wt% Fe_2O_3 calculated from the results of the chemical analysis and corresponds to (x = 1.5). These results show that the maximum substitution levels of Al_2O_3 by Fe_2O_3 varies a lot from one publication to another, probably because the synthesis protocols cannot be compared.

The presence of iron in the CSA cements also produces the ferritic phases. These phases are the major iron-containing phases in Ordinary Portland Cement (OPC) and also form in CSA cements. The ferritic phase represents a solid solution corresponding to the formula $Ca_2(Al_yFe_{2-y})O_5$ where y can vary from 0 to about 1.33 [16]. Crystal structures, chemical compositions and hydration of this phase are well known [16–22] and the substitution of Fe^{3+} by Al^{3+} in this phase causes structural variations [23].

Stoichiometric ye'elimite has orthorhombic symmetry at room temperature [24–26]. In another work [27], it was reported that the starting temperature of the orthorhombic-to-cubic

transformation during heating was 438 °C and that the reverse transformation during cooling occurred at 469 °C. However, a pseudocubic symmetry can be stabilized with the incorporation of foreign ions such as iron [8,12,24]. In a recent work [8], it was reported that the incorporation of iron in ye'elimite stabilizes its cubic polymorph at the expense of the orthorhombic one. In another study [4], a mixture of cubic and orthorhombic ye'elimite was found in commercial CSA clinkers, and just cubic ye'elimite in the borax-activated belite calcium sulfoaluminate clinker. Sodium and iron solid solutions have been prepared by Andaç et al. [24] to study the polymorphism of ye'elimite in the presence of these impurities. This study revealed a phase transformation; the polymorph of ye'elimite at high temperature is cubic, and pseudo-cubic at low temperature. A thermal quenching from a temperature higher than the structural transition temperature, and/or the addition of atoms forming solid-solution are usually two efficient techniques to stabilize a high-temperature polymorph.

1.3 Objective of the work: detailed microstructural study

As we can see from the published literature, the influence of iron on the crystallographic structure has been extensively studied. However, we did not find thorough studies presenting in details the effect of iron on the microstructure. The few available data mention the co-existence of ye'elimite and ferritic phases, as well as the presence of a liquid phase [3,9,16]. Nevertheless, the clear distinction between ye'elimite grains, calcium aluminate grains, ferritic phases and liquid phases has not been discussed or evidenced, and the particle size distribution has not been studied. To our opinion, a detailed microstructural study would help to visualize the spatial repartition of the different phases (crystallized and liquid phases) during the thermal treatment. The characterization of the microstructure is of interest to

follow the role of iron and to define the mechanisms of ye'elimite formation during thermal treatment.

The present work starts with a thorough description of the synthesis protocol of ye'elimite prepared with increasing quantities of iron. It is important to give all the experimental details because these pieces of information are often missing in the literature as we explained above. This paper continues with the description of the relation between iron oxide addition and the microstructural changes.

2. Materials and methods

2.1. Materials and sample preparation

The raw materials used for the sample preparation are $CaCO_3$, Al_2O_3, $CaSO_4.2H_2O$ and Fe_2O_3 (purity ≥ 99 wt%; supplier: Sigma-Aldrich). The quantities of iron oxide used, relative to the mass of all the raw materials, are: 0.00%, 1.01%, 2.01%, 2.53%, 5.11%, 10.44% and 21.38%. The prepared samples are noted respectively S0, S1, S2, S2.5, S5, S10 and S21. By assuming ideally that the added iron can substitute the aluminum in the structure of the ye'elimite, the theoretical formula of the doped ye'elimite is $C_4A_{3-x}F_x\bar{S}$. This formula assumes that all the iron is in the structure of the ye'elimite. In reality, we will see in the next sections of this paper that part of iron forms ferritic phases. The mass percentages of added Fe_2O_3 (wt% = 0.00%, 1.01%, 2.01%, 2.53%, 5.11%, 10.44% and 21.38%,) correspond, respectively, to values of x = 0.00, 0.05, 0.10, 0.12, 0.25, 0.53 and 1.13. Table 2 shows the amounts of raw materials used for the synthesized samples named from S0 to S21.

The following protocol has been used to prepare the samples: 100 g of the different mixtures were homogenized in a Turbula shaker mixer for 30 min and crushed in a planetary ball mills at 120 rpm for 1 h. Then 2.5 g of the homogenized mixture was uniaxially pressed into pellets, using a 16 mm cylindrical die, under a load of 1.5 tons. The heat treatment of the samples was carried out in a platinum crucible in an elevator furnace under air atmosphere and at 1300 °C (heating ramp: 5 °C/min, dwell duration: 3h, air quenching). This sintering cycle was chosen because it gave the highest percentage of pure ye'elemite.

2.2. Characterisation methods

Microscopic observations were performed on a JEOL IT300LV scanning electron microscope (SEM) equipped with an electron dispersive spectroscopy (EDS) detector for chemical analysis. The microscope was operated at 15 kV accelerating voltage. The preparation of the samples began with the preparation of a resin which contained 10 ml of epoxy (IP, PRESI France) and 1 ml of hardener (Catalyst, PRESI France). The samples were impregnated with the resin in a plastic container and deposited in a vacuum chamber for one hour. After solidification for 12 hours at ambient air, the samples were polished on Minitech 233 type machine (Presi, France), using SiC abrasive paper from P120, P240, P600, P1200, P2400 and P4000 rotated at 150 rpm. Polishing was performed according to the protocol described in Table 3. After polishing, samples were rinsed with ethanol in an ultrasonic bath for 15 minutes, then carbon-metallized to increase the surface conductivity during the SEM observations. For the observation of the powders, we used LEO 1530 V P field emission scanning electron microscopy (SEM) at a 3 kV accelerating voltage. Before observation, the powder was dispersed in absolute ethanol and a drop of the suspension was deposited on an aluminum support and dried in air.

The technique used to study the particle size distribution was image analysis (PSD-IA) using ImageJ V1.51 software. ImageJ is an image processing and analysis software. It allows to count the particles on SEM micrographs and to calculate the average diameter at a total of N particles (in the present work we have chosen N_{total} = 100). For each image, a standard deviation is also estimated. The average diameter of the calculated particle size distribution is as follows:

$$D = \frac{1}{100} \sum_{i=1}^{100} D_F$$

with D_F is the maximum Feret diameter; it represents the distance between the farthest points on the projection of each particle.

X-ray diffractions in this study were made by Bruker D8 Advance X-ray Diffractometer with CuKα radiation (λ_{Cu}=1.54056 Å, without monochromator) at a step scan of 0.02° with a time counting per step of 0.45 s operated at a voltage 40 kV and an electric current 40 mA. Analyzes were performed in a range of 2 theta between 5 and 55. The peaks corresponding to ye'elimite are indexed in Pcc2 orthorhombic space group, determined with the cell parameters a = 13.028(3) Å, b = 13.037(3) Å and c = 9.161(2) Å and in a cubic cell with space group I-43m with a = 9.2 Å. This lattice parameter refinement was carried out based on literature data; the theoretical spectra of the orthorhombic and cubic varieties of the ye'elimite are presented in Fig. 1. A semi-quantitative analysis of the mineral phases was carried out by considering the intensity of the most intense diffraction peak for each phase. In the case where ye'elimite was the dominant phase, a more precise quantification of the mineral phases was carried out by using Rietveld method in the TOPAS 4.2 software. In this instance, the adjustment parameters were: background coefficients, the zero-shift error, unit cell parameters. The pseudo-Voigt function was used for fitting the peaks. The ICSD

collection codes of the structures used for Rietveld refinement are given in Table 4 [19,28–34].

3. Results and discussion

3.1 Nature of the phases formed during the thermal treatment at 1300 °C for 3 h

The X-ray diffractograms for samples S0, S1, S2.5, S5, S10 and S21 treated at 1300 °C for 3 h are shown in Fig. 2. The results of the Rietveld analysis corresponding to samples S0, S1, S2.5, S5, S10 and S21 are given in Table 5.

In sample S0, the main phase is orthorhombic $C_4A_3\overline{S}$ ye'elimite which reaches 83.1 wt%, together with the formation of small amounts of calcium aluminates (krotite CA and grossite CA_2). Sample S1 (x = 0.05 in $C_4A_{3-x}F_x\overline{S}$) contained 98.7 wt% of ye'elimite $C_4A_{3-x}F_x\overline{S}$ in orthorhombic and cubic forms with the formation of minor phases CA and CA_2. For an addition of 1 wt% Fe_2O_3, the quantity of formed ye'elimite is significantly increased compared to the sample without iron, and some cubic polymorph is detected. This shows the effect of iron on the formation of ye'elimite and the effect of Fe^{3+} insertion in the crystal structure of ye'elimite. The presence of iron, even in small percentages, promotes the formation of iron bearing ye'elimite, and the substitution of the Fe^{3+} ions into ye'elimite causes the stabilization of the cubic polymorph at room temperature. When the iron concentration reached 2.5 wt% (case of sample S2.5 with x = 0.12), the ferritic phase $C_2(A,F)$ begins to appear. Fig. 3 zooms on the most intensive diffraction peak of this phase between 2θ = 11.8° and 12.5°; its diffraction intensity increases simultaneously with the increase in the percentage of added iron (Table 5). Our experimental results show that

beyond a certain quantity of iron (x = 0.12 in our case), Fe^{3+} can no longer enter into the ye'elimite structure. It forms a ferritic phase $C_2(A,F)$. The total ye'elimite content is almost constant in samples S1, S2.5 and S5 but the content of cubic ye'elimite increases with the increasing addition of iron. From composition S1 to S21, cubic ye'elimite increases at the expense of orthorhombic ye'elimite, which can be explained by the effect of Fe^{3+} ion substitution in the crystal structure where Fe^{3+} can replace Al^{3+} [8].

To conclude on this part, the solid-state synthesis protocol described in this study allowed to sinter at 1300 °C a clinker with large amounts of orthorhombic ye'elimite (~ 83.1 wt%) for the sample without iron, and more than 98 wt% of orth-$C_4A_3\overline{S}$ and cub-$C_4A_3\overline{S}$ for iron bearing sample with $0.05 \leq x \leq 0.25$ ($1.01\ \% \leq$ wt% $Fe_2O_3 \leq 5.11\%$). The ability of Fe^{3+} ions to enter the ye'elimite lattice and to replace Al^{3+} ions can influence the modification of its crystal structure. We can say that the incorporation of iron is complete when $x < 0.12$ (2.5 wt% of Fe_2O_3) and beyond x = 0.12, the ferritic phase $C_2(A,F)$ appears as a minor phase. The amount of ferritic phase increases with the addition of iron (Table 5), indicating that part of the iron is inserted inside ye'elimite phase and that the other part of the iron forms a secondary ferritic phase.

3.2 Effect of iron on the microstructure of compositions sintered at 1300 °C for 3h

The microstructure of the samples sintered at 1300 °C was studied using micrographs taken by SEM (Fig. 4). XRD data help us to decide which phases are detected by EDS analysis. Samples S0 without iron and S1 with a low iron content presents homogeneous and porous crystals of dark grey color which correspond, according to the EDS analysis, to ye'elimite $C_4A_3\overline{S}$ for S0 and iron bearing ye'elimite for S1. Micrographs and EDS analysis of S2.5, S5 and S10 show the presence of large proportions of ye'elimite and the formation of small

amounts of $C_2(A,F)$ (the crystals in light grey). $C_2(A,F)$ is quite distinguishable in sample S21. The amount of ferritic phase seems to increase from S5 to S21, which is consistent with the XRD observations. Appendix A presents the EDS spectra for the samples S0 to S21. On these spectra, we can see that EDS measurements carried out on ye'elimite type grains contain O, Al, S, Ca and a small percentage of iron in S1, S2.5, S5 (point A), S10 (point A) and S21 (point A). In samples S5, S10 and S21, the measurements on point B show a significant quantity of iron and no sulfur is present; therefore, these compositions correspond most certainly to the ferritic phase.

To identify the chemical elements and their distribution in the different samples, we carried out EDS mapping for each of S0, S1, S5, S10 and S21 samples (Fig. 5). EDS mapping of the S0 sample (x = 0) shows the elements corresponding to the $C_4A_3\overline{S}$ phase. The addition of iron oxide leads to the insertion of iron inside the ye'elimite phase $C_4A_{3-x}F_x\overline{S}$ for all synthesized samples, and the formation of ferritic phase $C_2(A,F)$ for ($x \geq 0.12$, i.e; 2.5 wt% of Fe_2O_3). Iron forms secondary ferritic phases (visible in the form of a mass) as soon as the added quantity is significant.

The microstructural changes in the presence of iron was assessed in detail. Fig. 6 shows the morphology of the powders S0, S1, S2.5, S5, S10 and S21 sintered for 3 h at 1300 °C. There is a clear distinction between the morphologies whether iron is present or not. The grains with a size of 2 µm and the grain boundaries are very distinct in the S0 sample. The grain morphology in samples S1, S2.5 and S5 tends to be more rounded, the grain boundaries between the particles are less clear than in S0, and the particles seem more interconnected. This may be due to the fluxing effect of the iron rich phase which promotes the cohesion and sintering between the grains. In samples S10 and S21, the grains grow and form densified clusters. This morphology can be explained by the presence of a liquid phase. It is well

known that the presence of iron oxide facilitates the formation of a liquid phase [9,14,16]. From these results, we can say that the fluxing effect of iron and the interaction of ye'elimite with the ferrous liquid phase are responsible for the modification of the grain morphology. For higher iron additions, iron leads to the formation of the ferritic phase and the formation of a ferrous liquid phase which results in the growth and densification of the grains.

We also finely examined the microstructure of the ferritic phases using micrographs taken by SEM. Representative morphologies are given in Fig. 7. Morphologies of needle shapes (Fig. 7a) or in the form of continuous massive interstitial phase (Fig. 7b) can be distinguished. Such dendritic forms have been observed in Portland cements [35,36], but very rarely in CSA cements to our knowledge [16]. The ferritic phase occurring in Portland cements represents an interstitial phase and may occur as a dendritic form. In the literature, some authors [35,36] have suggested that the ferritic phase occurs with both massive forms and dendritic patterns in Portland cements. According to [35], rapid cooling can result in the conversion of interstitial phases such as the ferritic phase into the dendritic structure. Touzo et al. [16] shows the presence of an interstitial material composed of needles and dendrites in CSA cement; the needles represent a secondary ferritic phase which had crystallized from the melt. In our case, the difference between the two forms of ferritic phase is clear in the iron rich compositions. It suggests that during cooling of ye'elimite based compositions, part of the melt remains in the form of continuous massive interstitial phase, and another part transforms into crystals in the form of needles.

3.3 Evolution of the microstructure as a function of sintering duration (0 to 180 min) at 1300 °C for a given quantity of iron oxide

After the examination of the microstructures of the samples as a function of the percentage of added iron, it is interesting to study the evolution and the microstructural changes of the phases as a function of dwell time at 1300 °C for the formation of ye'elimite. In this respect, we have chosen to follow the microstructural changes in the sample S10 (x = 0.53, i.e; 10.44 wt% of Fe_2O_3) sintered at 1300 °C for different durations from 0 to 180 min and without any intermediate grinding step.

First, a mineralogical analysis was performed to identify the phases. The X-ray diffractograms of sample S10 sintered at 1300 °C during different durations are presented in Fig. 8. The following comments can be made:

(i) The diffraction peaks associated to Al_2O_3, $CaSO_4$, CA, CA_2, ye'elimite and ferritic phase are detected at 1300 °C for the dwell time 0 s.

(ii) By increasing the dwell time from 15 min to 30 min, the peaks of Al_2O_3, $CaSO_4$ and CA_2 are attenuated and after sintering for 1h, these phases disappear.

(iii) After a 3h sintering, and after the consumption of the phases by the reactions between calcium aluminates (CA and CA_2) and $C\overline{S}$, ye'elimite becomes the main phase with the presence of ferritic phase.

Fig. 9 shows the EDS mapping of the backscattered electron images of the phases observed during the formation of ye'elimite as a function of dwell time. Fig. 10 shows the composition profiles obtained by EDS analysis, presenting the elemental percentages of calcium, aluminum, sulfur, iron and oxygen along the red lines drawn on the micrographs of the sample S10. Fig. 9a shows the colored mapping of sample S10 sintered at 1300 °C for dwell time of 0 seconds, which means that the sample was immediately quenched when the furnace reached 1300 °C. From the EDS data, Al_2O_3, CA_2, CA, ye'elimite and ferritic phase were detected in this microstructural observation. Al_2O_3 grains are surrounded by CA_2 and

CA. Some EDS points indicate that a very thin layer of CA_6 possibly surrounds Al_2O_3 and is itself surrounded by CA_2 (Fig. 10a). Ye'elimite was formed around the calcium aluminate phase. The ferritic phase is formed in some regions. By increasing the dwell time to 15 min (Fig. 9b and 10b), the core of alumina grains reduces considerably and the calcium aluminate layer thickens as well as the external layer of ye'elimite. After a longer sintering duration (30 min and 60 min, Fig. 9c and Fig. 9d), we notice that the Al_2O_3 grains disappear and only CA remains in the center of the grains surrounded by ye'elimite and small amounts of ferritic phase on the edges (Fig. 10c). Finally, for the sample sintered for 180 min, the CA phase disappears and the formation of the ye'elimite is complete. The ye'elimite grains are surrounded by an iron rich liquid phase (Fig. 9e and Fig. 10d).

From SEM and EDS observations, we can assume that Ca^{2+} ions are diffusive species that react with alumina to form CA_2; it causes a decrease in the grain size of Al_2O_3 (Fig. 9b). Ca^{2+} ions can also react with CA_2 to produce CA; this may explain the consumption of CA_2 and the growth of the CA layer (Fig. 9c). The calcium aluminate fraction is composed of CA and CA_2 until a sintering duration of 15 min at 1300 °C. Beyond this duration, Grossite CA_2 is totally consumed to form Krotite CA. For longer sintering times (≥ 60min), CA can react with $C\overline{S}$ and eventually transform into ye'elimite.

The presence of iron in the sample seems to have two effects. The first effect can be seen by comparing our work in this section with [37] which studied the phenomena of ye'elimite formation in a pure system as a function of the dwell time at 1300 °C. We can deduce by this comparison that the total consumption of Al_2O_3 and CA_2 takes place in the sample containing iron at shorter sintering duration than in the pure system. The presence of iron seems to facilitate the formation of CA and allows more time for all the CA grains to convert into ye'elimite; the consequence is the formation of a higher amount of ye'elimite containing iron (92.1 wt% of ye'elimite in S10 compared to 83.1 wt% in S0) at 1300 °C for

180 min. The second effect of iron is its high concentration observed at the edges of the grains. It is associated with the formation of a layer of ferritic phase that surrounds the ye'elimite and calcium aluminate grains.

A close observation of the polished sections of S10 and of the EDS analysis (Fig. 11) shows a clear distinction between Krotite CA grains (light grey) and ye'elimite grains (dark grey) in the S10 sample sintered at 1300 °C for 60 min. The zooms show the faceted morphology of CA and ye'elimite grains and the presence of a liquid phase allowing contact between the grains (Fig. 11a). The faceting of the grains and the presence of the liquid phase may be an indication of a liquid phase sintering mechanism as we already assumed. The liquid phase sintering takes place by the phenomena of dissolution-precipitation which consists in the fast transport of matter by diffusion. The consequence is the grain growth and the faceting of grains, the total and fast consumption of alumina and intermediate phases (calcium aluminates) for the formation of ye'elimite [9]. By increasing the sintering time to 3h, all the CA grains disappear and the faceted grains of the ye'elimite grow; Fig. 11b shows large grains of ye'elimite alone surrounded by a liquid phase film.

The changes of grain sizes of ye'elemite and krotite as a function of sintering duration was studied by image analysis (PSD-IA) using Image J V1.51 software. Fig. 12 shows the monomodal particle size distribution of krotite CA (crystals in light gray) and ye'elimite (crystals in dark gray) in the S10 sample treated at 1300 °C for different durations: 30 min, 60 min and 180 min. The mean particle diameters of the PSD-IA distribution of ye'elimite are 2.19 µm, 2.88 µm and 7.76 µm respectively for sintering times of 30 min, 60 min and 180 min. The mean particle diameters of krotite CA are 5.20 µm and 3.22 µm respectively for sintering times of 30 min and 60 min. Beyond this time, the CA grains disappear. The CA grains are in the center surrounded by the small ye'elimite grains. By increasing the sintering time, the CA grains progressively decrease in size and are totally replaced by large

grains of ye'elimite after 3h of sintering. When the grains are of the same nature, the liquid phase sintering promotes the mechanisms of dissolution of the fine grains and their precipitations on the larger ones.

4. Conclusion

The present study describes the effect of iron on the microstructure of ye'elimite and minor phases, based on SEM, EDS observations together with XRD analysis. The raw materials were Al_2O_3, CaO, $CaSO_4$ and Fe_2O_3. The quantities of iron oxide used, relative to the mass of all the raw materials, are: 0.00%, 1.01%, 2.01%, 2.53%, 5.11%, 10.44% and 21.38%. The chosen sintering temperature was 1300 °C.

Fig. 13 summarizes schematically the results of the microstructural study. Fig. 13a sketches the evolution of phases and microstructure as a function of the percentage of iron oxide in the samples. The ferritic phase appears at 2.5 wt% of Fe_2O_3. By increasing the percentage of iron oxide in the samples, the amount of ferritic phase also increases and develops two different morphologies during cooling: a melt morphology and needle-like crystals. In the ye'elimite without iron, the contours of the grains are well distinguished. As the percentage of iron increases, the particles appear more interconnected and the consequence is growth of the grains. Fig. 13b sketches the evolution of phases and microstructure as a function of the sintering time in sample S10 (x = 0.53, i.e; 10.44 wt% of Fe_2O_3) at 1300 °C. The microstructure forms in several layers of phases going from Al_2O_3 grains to ye'elimite, through CA_2 and CA, and a weak external layer of ferritic phase. Alumina reacts with Ca^{2+} to produce CA_2, and grossite is transformed into CA which in turn reacts with S^{VI+} and is totally converted into ye'elimite. Our microscopic observations report for the first time a clear distinction between calcium aluminate grains and ye'elimite grains. Calcium

aluminates CA are presented as faceted grains surrounded by small grains of ye'elimite and an iron-rich liquid phase. The phase transformations take place thanks to the diffusion mechanisms provided by the ferritic liquid phase which favors the dissolution-precipitation of the CA grains to form large grains of ye'elimite.

Acknowledgments

The authors would like to thank the University of Limoges and the University of Marrakech for funding Fatima Z. ABIR's PhD scholarship.

References

[1] F.P. Glasser, L. Zhang, High-performance cement matrices based on calcium sulfoaluminate–belite compositions, Cem. Concr. Res. 31 (2001) 1881–1886. https://doi.org/10.1016/S0008-8846(01)00649-4.

[2] H.-M. Ludwig, W. Zhang, Research review of cement clinker chemistry, Cem. Concr. Res. 78 (2015) 24–37. https://doi.org/10.1016/j.cemconres.2015.05.018.

[3] M. Idrissi, A. Diouri, D. Damidot, J.M. Greneche, M.A. Talbi, M. Taibi, Characterisation of iron inclusion during the formation of calcium sulfoaluminate phase, Cem. Concr. Res. 40 (2010) 1314–1319. https://doi.org/10.1016/j.cemconres.2010.02.009.

[4] G. Álvarez-Pinazo, A. Cuesta, M. García-Maté, I. Santacruz, E.R. Losilla, A.G. De la Torre, L. León-Reina, M.A. Aranda, Rietveld quantitative phase analysis of Yeelimite-containing cements, Cem. Concr. Res. 42 (2012) 960–971. https://doi.org/10.1016/j.cemconres.2012.03.018.

[5] F. Winnefeld, S. Barlag, Calorimetric and thermogravimetric study on the influence of calcium sulfate on the hydration of ye'elimite, J. Therm. Anal. Calorim. 101 (2010) 949–957. https://doi.org/10.1007/s10973-009-0582-6.

[6] E. Gartner, T. Sui, Alternative cement clinkers, Cem. Concr. Res. 114 (2018) 27–39. https://doi.org/10.1016/j.cemconres.2017.02.002.

[7] Y. Li, X. Liu, X. Niu, L. Song, Influence of minor oxides on formation and decomposition of mineral calcium sulfoaluminate ($3CaO.3Al_2O_3.CaSO_4$), Mater. Res. Innov. 11 (2007) 92–94. https://doi.org/10.1179/143307507X196644.

[8] F. Bullerjahn, D. Schmitt, M. Ben Haha, Effect of raw mix design and of clinkering process on the formation and mineralogical composition of (ternesite) belite calcium sulphoaluminate ferrite clinker, Cem. Concr. Res. 59 (2014) 87–95. https://doi.org/10.1016/j.cemconres.2014.02.004.

[9] F. Bullerjahn, T. Scholten, K.L. Scrivener, M. Ben Haha, A. Wolter, Formation, composition and stability of ye'elimite and iron-bearing solid solutions, Cem. Concr. Res. 131 (2020) 106009. https://doi.org/10.1016/j.cemconres.2020.106009.

[10] F. Bullerjahn, M. Zajac, M. Ben Haha, K.L. Scrivener, Factors influencing the hydration kinetics of ye'elimite; effect of mayenite, Cem. Concr. Res. 116 (2019) 113–119. https://doi.org/10.1016/j.cemconres.2018.10.026.

[11] D. Chen, X. Feng, S. Long, The influence of ferric oxide on the properties of $3CaO.3Al_2O_3.CaSO_4$, Thermochim. Acta. 215 (1993) 157–169. https://doi.org/10.1016/0040-6031(93)80089-S.

[12] A. Cuesta, A.G. De la Torre, E.R. Losilla, I. Santacruz, M.A. Aranda, Pseudocubic crystal structure and phase transition in doped ye'elimite, Cryst. Growth Des. 14 (2014) 5158–5163. https://doi.org/10.1021/cg501290q.

[13] J. Strigáč, M.T. Palou, J. Krištin, J. Majling, Morphology and chemical composition of minerals inside the phase assemblage $C\text{-}C_2S\text{-}C_4A_3S\text{-}C_4AF\text{-}CS$ relevant to sulphoaluminate belite cements, Ceram.-Silikáty. 44 (2000) 26–34. https://www.irsm.cas.cz/materialy/cs_content/2000/Strigac_CS_2000_0000.pdf

[14] N. Zupancic, D. Kolar, D. Susnik, Z. Samardzija, Role of Fe_2O_3 on formation kinetics and microstructure of calcium sulphoaluminoferrite $C_4(A,F)_3s$, Br. Ceram. Trans. 93 (1994) 219–223.

[15] J.S. Ndzila, S. Liu, G. Jing, S. Wang, Z. Ye, The effect of Fe^{3+} ion substitution on the crystal structure of ye'elimite, Ceram.-Silikáty. 64 (2020) 18–28. https://doi: 10.13168/cs.2019.0044.
[16] B. Touzo, K.L. Scrivener, F.P. Glasser, Phase compositions and equilibria in the CaO–Al_2O_3–Fe_2O_3–SO_3 system, for assemblages containing ye'elimite and ferrite $Ca_2(Al,Fe)O_5$, Cem. Concr. Res. 54 (2013) 77–86. https://doi.org/10.1016/j.cemconres.2013.08.005.
[17] W.C. Hansen, L.T. Brownmiller, R.H. Bogue, Studies on the System Calcium oxide-alumina-ferric oxide[1], J. Am. Chem. Soc. 50 (1928) 396–406. https://doi.org/10.1021/ja01389a023.
[18] A.A. Colville, S. Geller, The crystal structure of brownmillerite, Ca_2FeAlO_5, Acta Crystallogr. B 27 (1971) 2311–2315. https://doi.org/10.1107/S056774087100579X.
[19] A.A. Colville, S. Geller, Crystal structures of $Ca_2Fe_{1.43}Al_{0.57}O_5$ and $Ca_2Fe_{1.28}Al_{0.72}O_5$, Acta Crystallogr. B 28 (1972) 3196–3200. https://doi.org/10.1107/S0567740872007733.
[20] J.M. Fortune, J.M.D. Coey, Hydration products of calcium aluminoferrite, Cem. Concr. Res. 13 (1983) 696–702. https://doi.org/10.1016/0008-8846(83)90060-1.
[21] T. Liang, Y. Nanru, Hydration products of calcium aluminoferrite in the presence of gypsum, Cem. Concr. Res. 24 (1994) 150–158. https://doi.org/10.1016/0008-8846(94)90096-5.
[22] A. Cuesta, I. Santacruz, S.G. Sanfélix, F. Fauth, M.A.G. Aranda, A.G. De la Torre, Hydration of C_4AF in the presence of other phases: A synchrotron X-ray powder diffraction study, Constr. Build. Mater. 101 (2015) 818–827. https://doi.org/10.1016/j.conbuildmat.2015.10.114.
[23] G.J. Redhammer, G. Tippelt, G. Roth, G. Amthauer, Structural variations in the brownmillerite series $Ca_2(Fe_{2-x}Al_x)O_5$: Single-crystal X-ray diffraction at 25° C and high-temperature X-ray powder diffraction (25° C ≤ T ≤ 1000° C), Am. Mineral. 89 (2004) 405–420. https://doi.org/10.2138/am-2004-2-322.
[24] O. Andac, F.P. Glasser, Polymorphism of calcium sulphoaluminate ($Ca_4Al_6O_{16}.SO_3$) and its solid solutions, Adv. Cem. Res. 6 (1994) 57–60. https://doi.org/10.1680/adcr.1994.6.22.57.
[25] A. Cuesta, A.G. De la Torre, E.R. Losilla, V.K. Peterson, P. Rejmak, A. Ayuela, C. Frontera, M.A. Aranda, Structure, atomistic simulations, and phase transition of stoichiometric yeelimite, Chem. Mater. 25 (2013) 1680–1687. https://doi.org/10.1021/cm400129z.
[26] Y. El Khessaimi, Y. El Hafiane, A. Smith, R. Trauchessec, C. Diliberto, A. Lecomte, Solid-state synthesis of pure ye'elimite, J. Eur. Ceram. Soc. 38 (2018) 3401–3411. https://doi.org/10.1016/j.jeurceramsoc.2018.03.018.
[27] D. Kurokawa, S. Takeda, M. Colas, T. Asaka, P. Thomas, K. Fukuda, Phase transformation of $Ca_4[Al_6O_{12}]SO_4$ and its disordered crystal structure at 1073K, J. Solid State Chem. 215 (2014) 265–270. https://doi.org/10.1016/j.jssc.2014.03.040.
[28] N.J. Calos, C.H. Kennard, A.K. Whittaker, R.L. Davis, Structure of calcium aluminate sulfate $Ca_4Al_6O_{16}S$, J. Solid State Chem. 119 (1995) 1–7. https://doi.org/10.1016/0022-4596(95)80002-7.
[29] H. Saalfeld, W. Depmeier, Silicon-Free Compounds with Sodalite Structure, Krist. Tech. 7 (1972) 229–233. https://doi.org/10.1002/crat.19720070125.
[30] W. Hörkner, H.K. Müller-Buschbaum, Crystal-structure of $CaAl_2O_4$, J. Inorg. Nucl. Chem. 38 (1976) 983–984. https://doi.org/10.1016/0022-1902(76)80011-5

[31] P.J. Baldock, A. Parker, I. Sladdin, X-ray powder diffraction data for calcium monoaluminate and calcium dialuminate, J. Appl. Crystallogr. 3 (1970) 188–191. https://doi.org/10.1107/S0021889870005952.
[32] A. Kirfel, G. Will, Charge density in anhydrite, $CaSO_4$, from X-ray and neutron diffraction measurements, Acta Crystallogr. B. 36 (1980) 2881–2890. https://doi.org/10.1107/S0567740880010461.
[33] I. Oftedal, Die Gitterkonstanten von CaO, CaS, CaSe, CaTe, Z. Für Phys. Chem. 128U (1927) 154–158. https://doi.org/10.1515/zpch-1927-12810.
[34] E.N. Maslen, V.A. Streltsov, N.R. Streltsova, N. Ishizawa, Y. Satow, Synchrotron X-ray study of the electron density in α-Al_2O_3, Acta Crystallogr. B. 49 (1993) 973–980. https://doi.org/10.1107/S0108768193006901.
[35] B. Felekoğlu, K. Tosun, B. Baradan, A. Altun, Effects of porosity and related interstitial phase morphology difference on the grindability of clinkers, Mater. Struct. 43 (2010) 179–193. https://doi.org/10.1617/s11527-009-9479-x.
[36] B. Felekoğlu, K. Tosun, B. Baradan, A. Altun, Relationship between clinker porosity and interstitial phase morphology, Adv. Cem. Res. 20 (2008) 109–119. https://doi.org/10.1680/adcr.2008.20.3.109.
[37] Y. El Khessaimi, Y. El Hafiane, A. Smith, Examination of ye'elimite formation mechanisms, J. Eur. Ceram. Soc. 39 (2019) 5086–5095. https://doi.org/10.1016/j.jeurceramsoc.2019.07.042.

Figure captions

Fig. 1.	XRD theoretical spectra of the orthorhombic and cubic ye'elimite; Cub-Y = Cubic Ye'elimite with ICSD-code 9560, Orth-Y = Orthorhombic Ye'elimite with ICSD-code 80361.
Fig. 2.	XRD diagrams of samples S0, S1, S2.5, S5, S10 and S21 heat-treated at 1300 °C for3 h. Symbols: Y=Ye'elimite, G=Grossite, K=Krotite, F=Ferritic phase.
Fig. 3.	Zoom on the ferritic phase $C_2(A,F)$ peak between 11.8 and 12.5° (2θ) in samples S1, S2, S2.5, S5, S10 and S21 calcined at 1300 °C.
Fig. 4.	SEM micrograph of sample S0, S1, S2.5, S5, S10 and S21 sintered for 3 h at 1300 °C, with spectra of the EDS analysis. The corresponding EDS point analyses with atomic percentages are presented in Appendix A.
Fig. 5.	EDS mapping presenting the distribution of different elements O, Ca, S, Al and Fe in samples S0 to S21.
Fig. 6.	Micrographs of powders S0, S1, S2.5, S5, S10 and S21 sintered for 3 h at 1300 °C
Fig. 7.	Representative micrographs of ferritic phase in sample S21 with different morphologies: dendritic (a), phase structure as a melt (b). Symbols: Y=Ye'elimite, F=Ferritic phase.
Fig. 8.	XRD diagrams of sample S10 heat-treated at 1300 °C different durations: 0 min, 15 min, 30 min, 60 min, and 180 min. Symbols: Y=Ye'elimite, G=Grossite, K=Krotite, F=Ferritic phase, A=Alumina, $C\overline{S}$=Calcium sulfate.
Fig. 9.	EDS mapping of elements present in sample S10 treated at 1300 °C for different durations: 0 min (a), 15 min (b), 30 min (c), 60 min (d), and 180 min (e). Symbols: Y=Ye'elimite, CA_2=Grossite, CA=Krotite, F=Ferritic phase, A=Alumina, $C\overline{S}$=Calcium sulfate.
Fig. 10.	EDS mapping presenting the distribution of all elements and composition profiles obtained by EDS analysis, presenting the atomic percentages of the elements Ca, Al, S, Fe and O as a function of the location along the red lines drawn on the micrographs of the sample S10 treated at 1300 °C for different durations: 0 min (a), 15 min (b), 60 min (c), and 180 min (d).
Fig. 11.	SEM micrographs of the S10 sample sintered at 1300 °C for 60 min (a) and 180 min (b). The zooms show the distinction between the faceted grains of ye'elimite and CA resulting from liquid phase sintering. The corresponding EDS point analyses for each phase are shown.
Fig. 12.	SEM micrographs of the S10 sample sintered at 1300 °C for 30 min, 60 min and 180min. The particle size distribution of CA and ye'elimite grains was examined by PSD-IA from a total of 100 particles to determine the average diameter and deviation.
Fig. 13.	Schematic representation of microstructural development of the phases according to the percentage of Fe_2O_3 (a) and of the microstructural development of the phases in the presence of iron, according to the sintering

	time at 1300 °C (b).
Appendix A	Typical EDS spectra of samples shown in fig. 4.
Table 1	Summary of synthesis conditions described in previous works for solid-state synthesis of ye'elimite. (*) x represents the number of moles of substitution of Al_2O_3 by Fe_2O_3.
Table 2	Amounts (wt. %) of the raw materials to prepare S0-S21 samples.
Table 3	Polishing protocol for samples prepared in resin.
Table 4	ICSD collection codes for phases used in the Rietveld analysis quantification
Table 5	Quantitative Rietveld analysis of phases in samples S0, S1, S2.5, S5, S10 and S21 heat-treated at 1300 °C. The values in brackets correspond to the error by the quantitative Rietveld analysis. (*) Rwp is the weighted profile factor and Rexp is the expected factor.

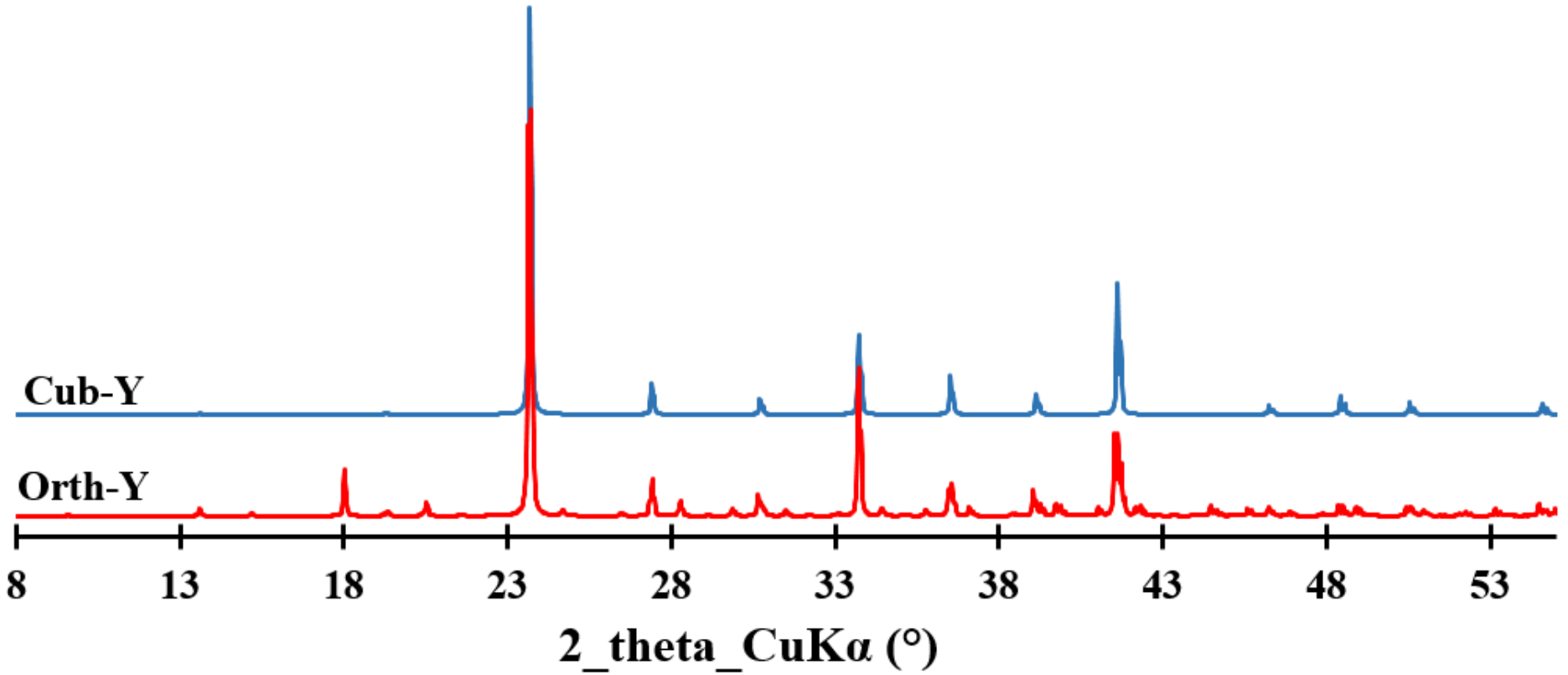

Fig. 1. XRD theoretical spectra of the orthorhombic and cubic ye'elimite; Cub-Y = Cubic Ye'elimite with ICSD-code 9560, Orth-Y = Orthorhombic Ye'elimite with ICSD-code 80361.

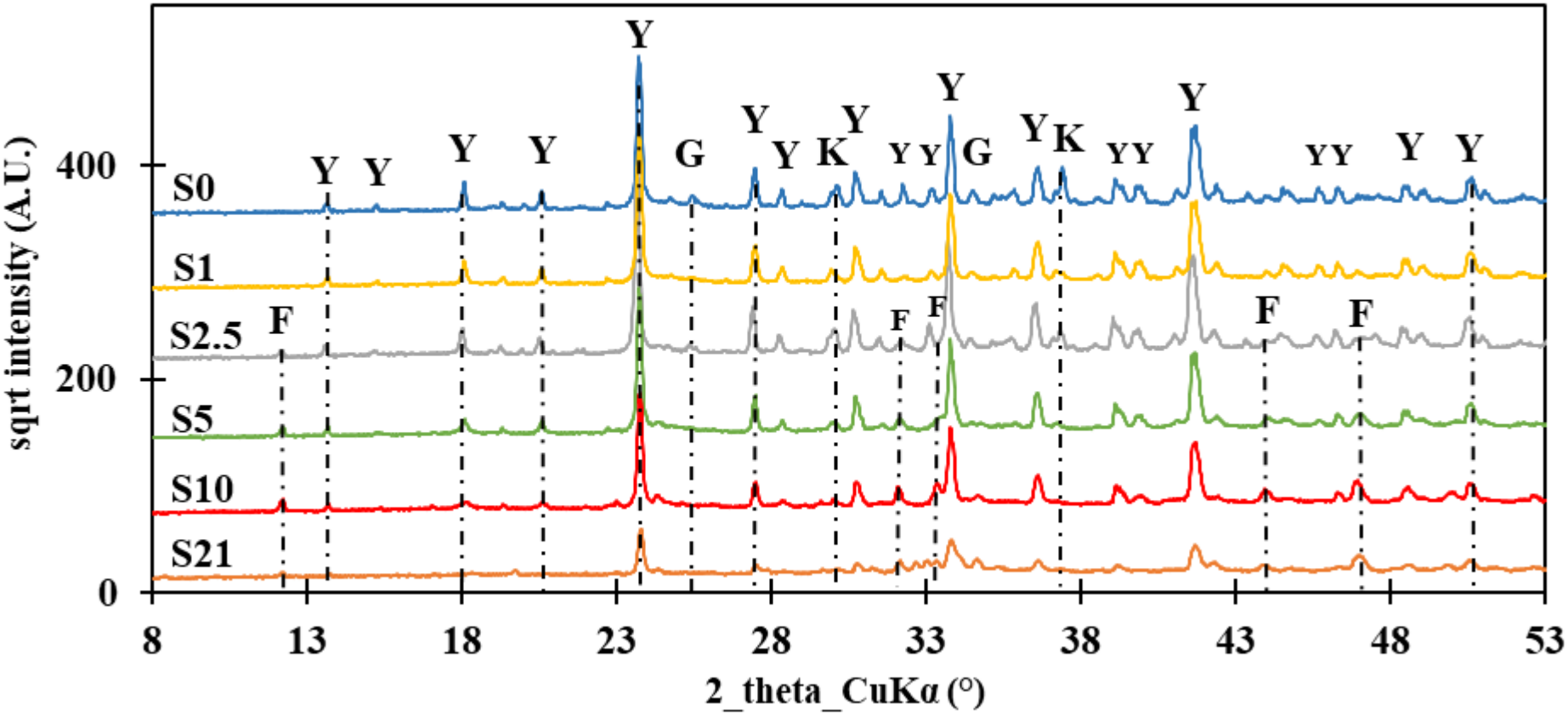

Fig. 2. XRD diagrams of samples S0, S1, S2.5, S5, S10 and S21 heat-treated at 1300 °C for 3 h. Symbols: Y=Ye'elimite, G=Grossite, K=Krotite, F=Ferritic phase.

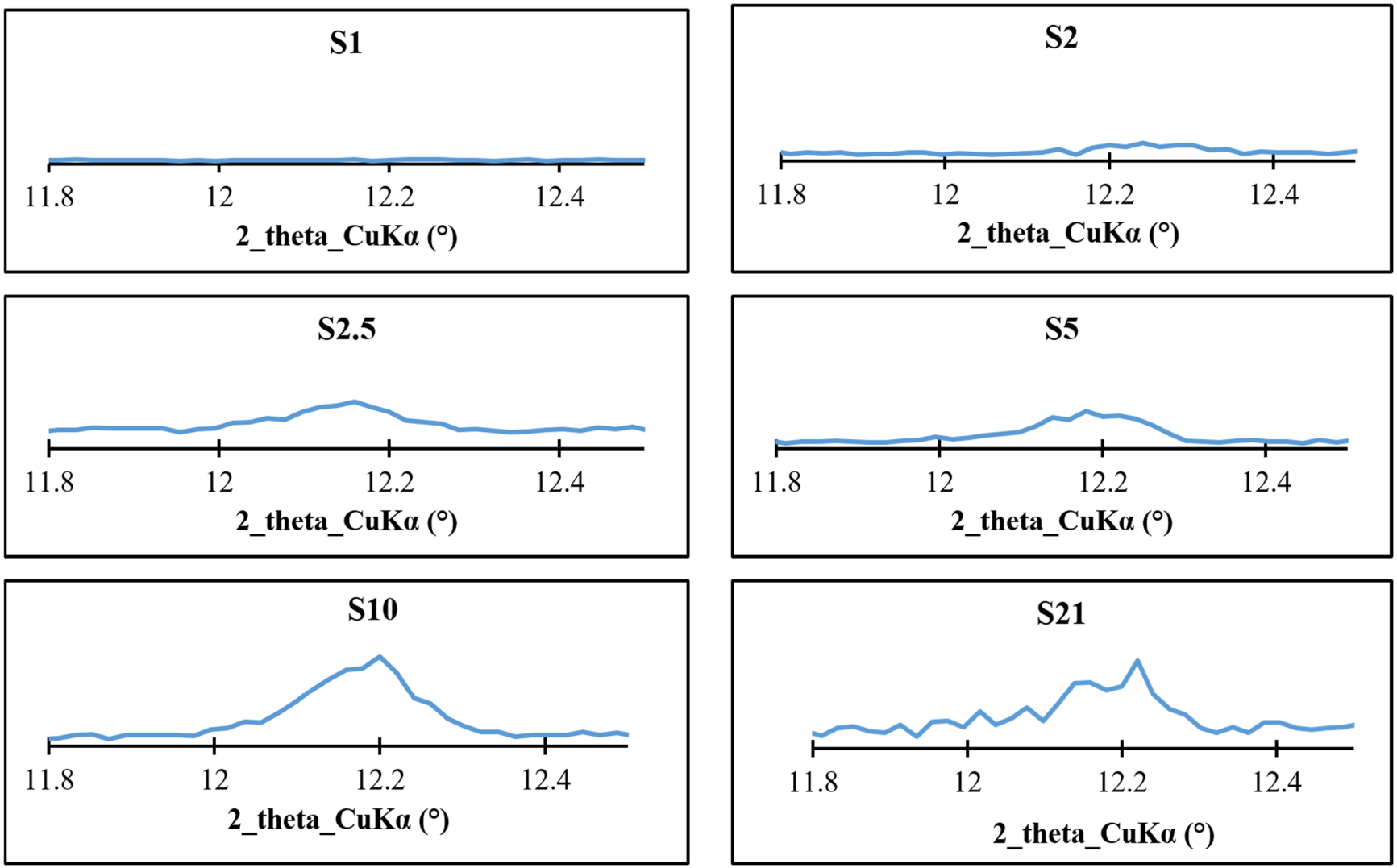

Fig. 3. Zoom on the ferritic phase C_2(A,F) peak between 11.8 and 12.5° (2θ) in samples S1, S2, S2.5, S5, S10 and S21 heat treated at 1300 °C for 3 h.

S0	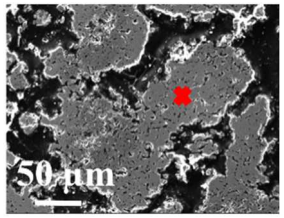	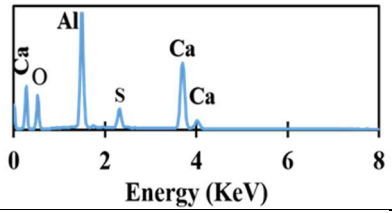	
S1	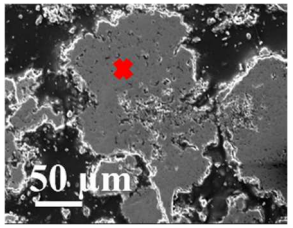	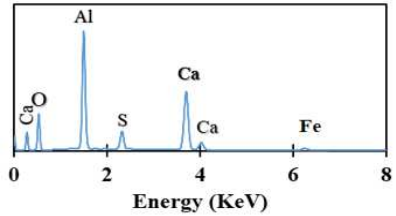	
S2.5	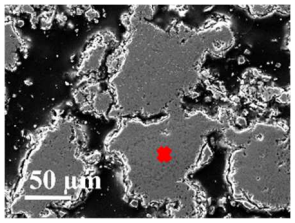	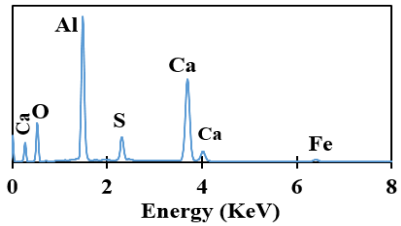	
S5	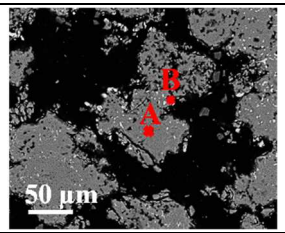	Point A 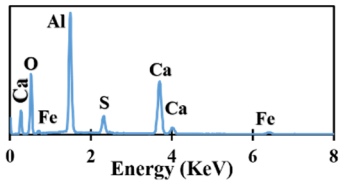	Point B 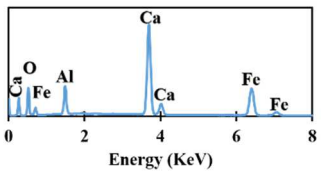
S10	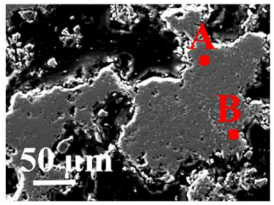	Point A 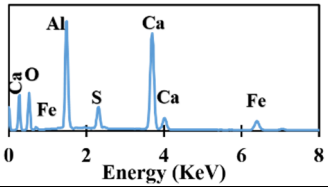	Point B 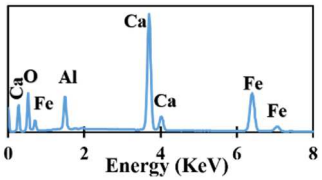
S21	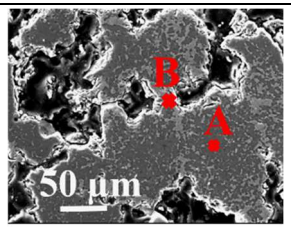	Point A 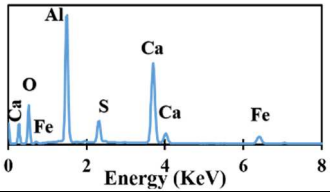	Point B 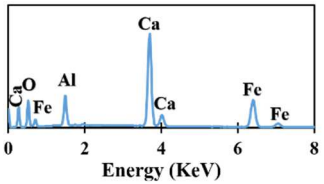

Fig. 4. SEM micrograph of sample S0, S1, S2.5, S5, S10 and S21 heat treated for 3 h at 1300 °C, with spectra of the EDS analysis. The corresponding EDS point analyses with atomic percentages are presented in Appendix A.

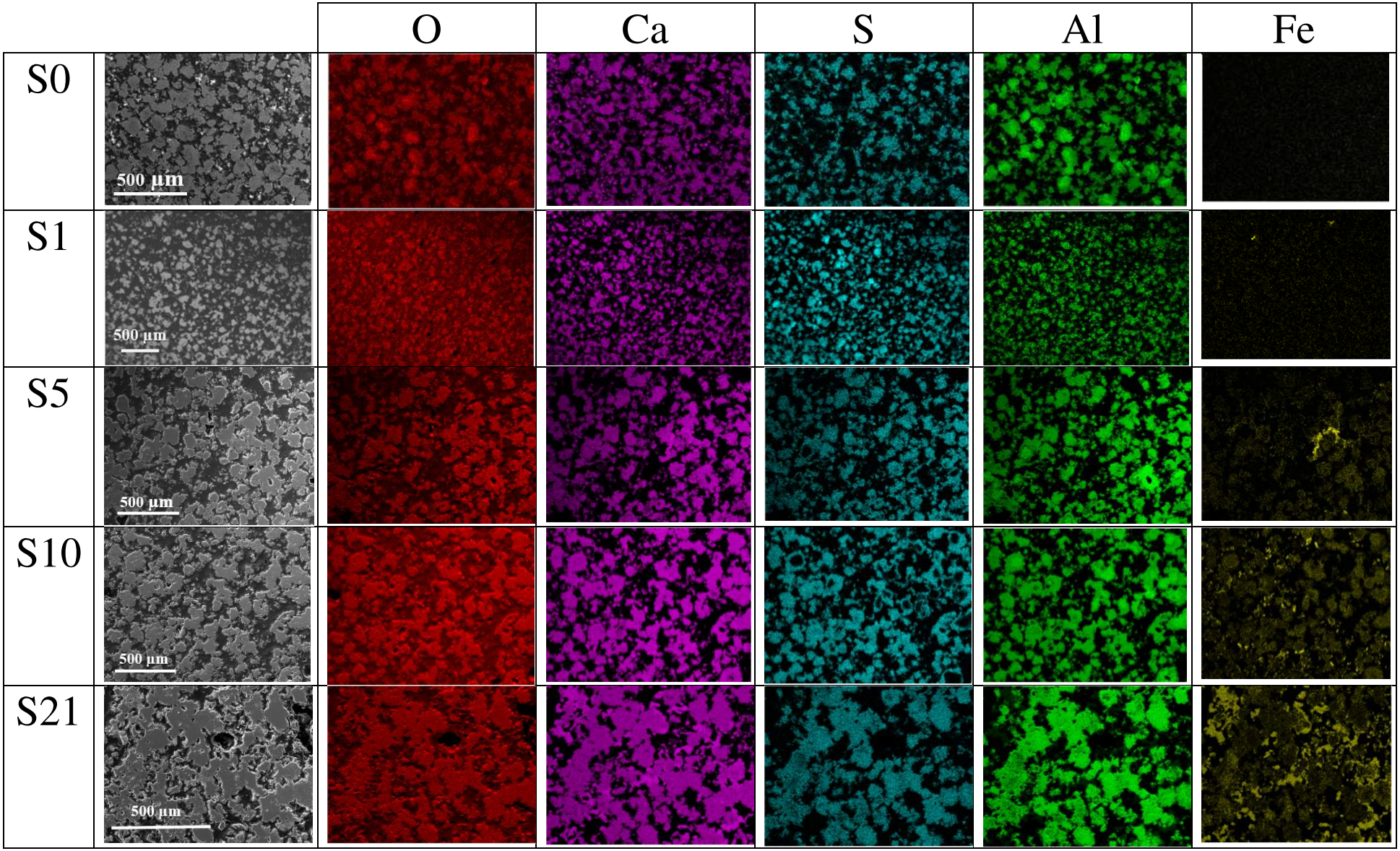

Fig. 5. EDS mapping presenting the distribution of different elements O, Ca, S, Al and Fe in samples S0 to S21.

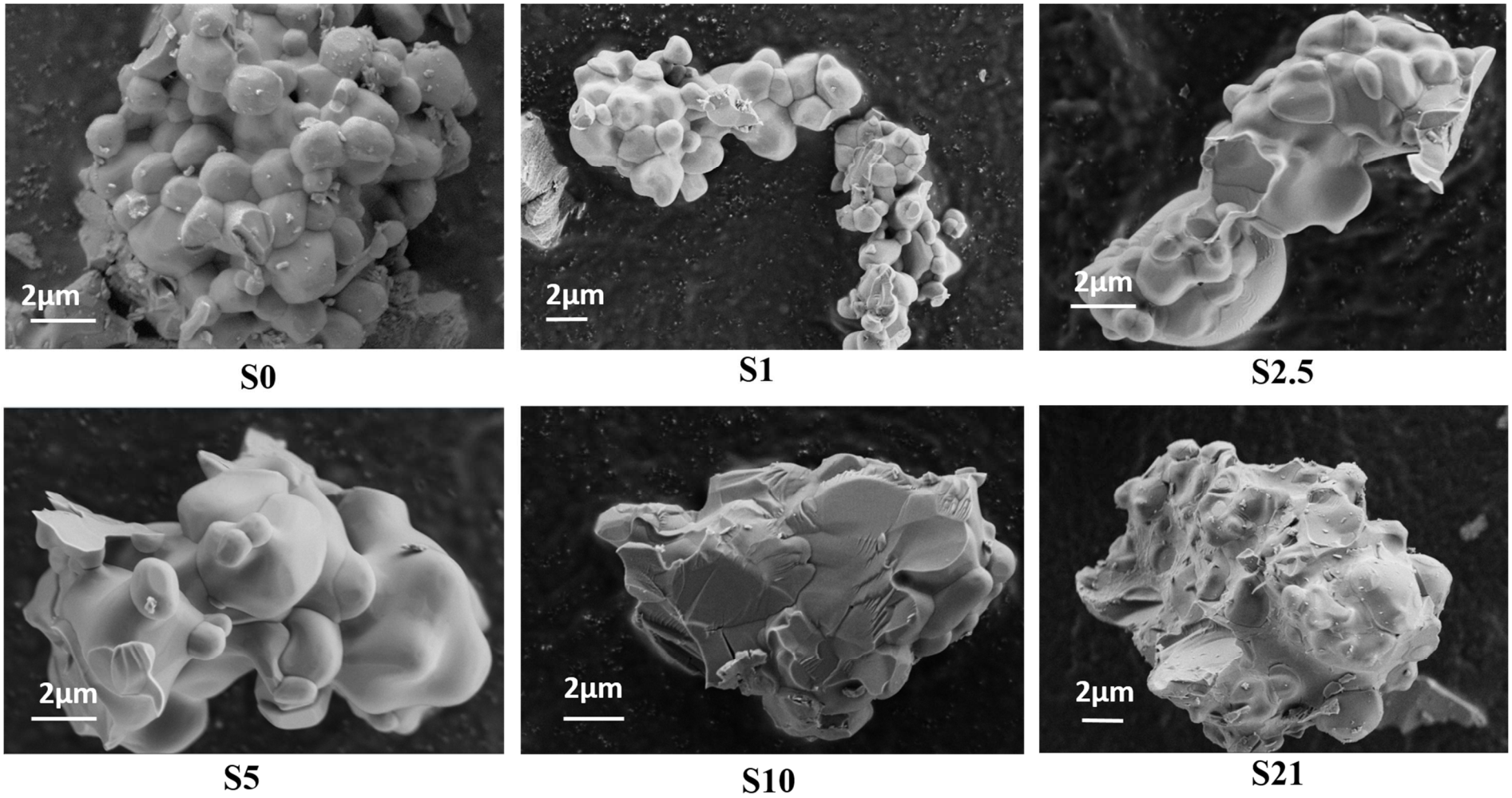

Fig. 6. Micrographs of powders S0, S1, S2.5, S5, S10 and S21 heat treated for 3 h at 1300 °C

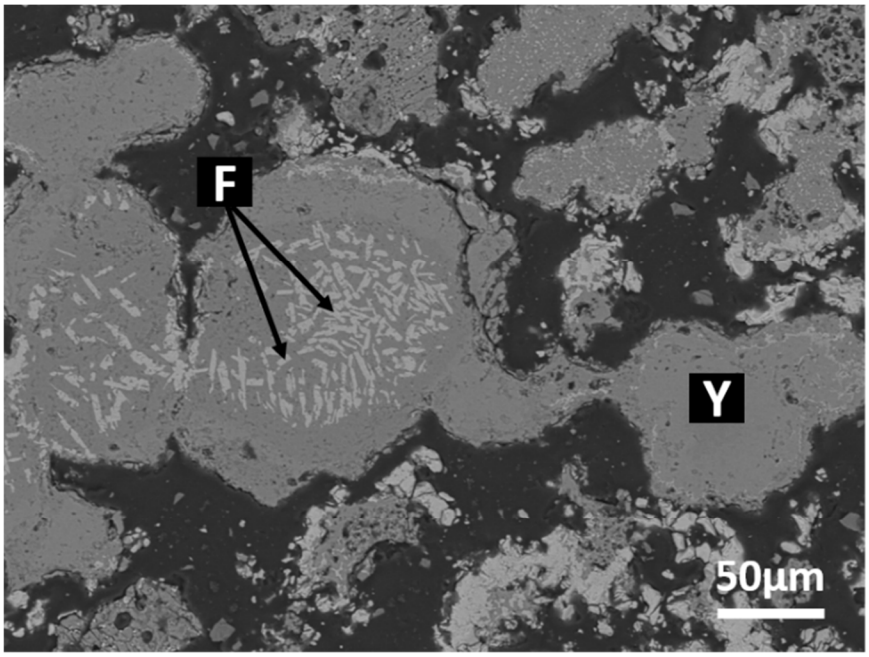

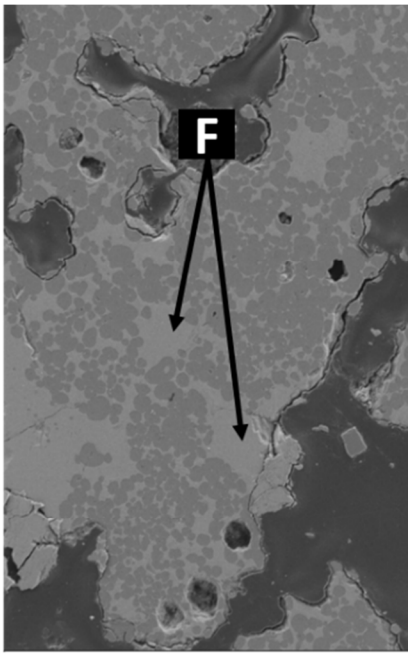

(a)

Fig. 7. Representative micrographs of ferritic phase in sample S21 with different morphologies: dendritic
Symbols: Y=Ye'elimite, F=Ferritic phase.

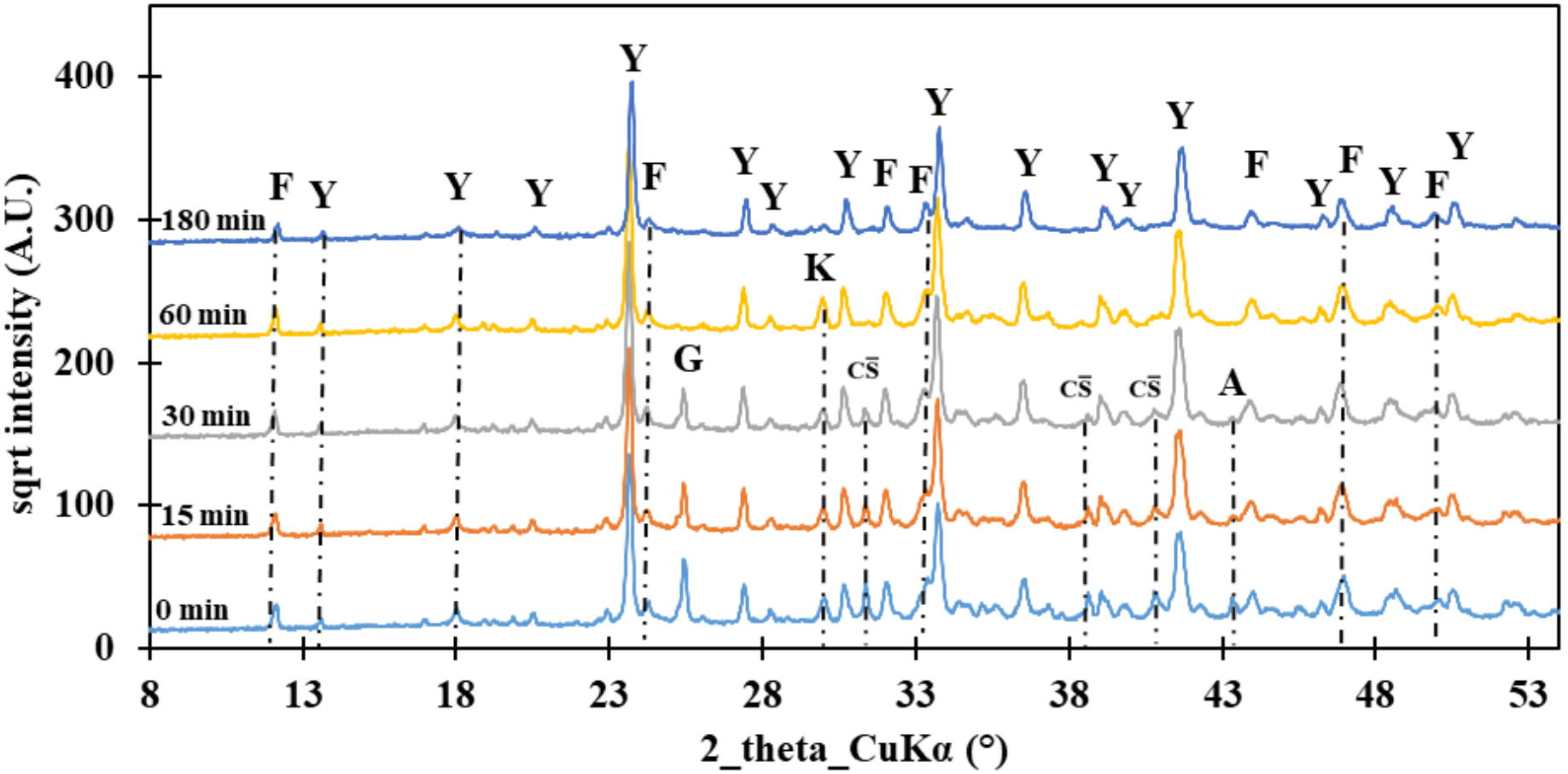

Fig. 8. XRD diagrams of sample S10 heat-treated at 1300 °C different durations: 0 min, 15 min, 30 min, 60 min, and 180 min. Symbols: Y=Ye'elimite, G=Grossite, K=Krotite, F=Ferritic phase, A=Alumina, C$\bar{S}$=Calcium sulfate.

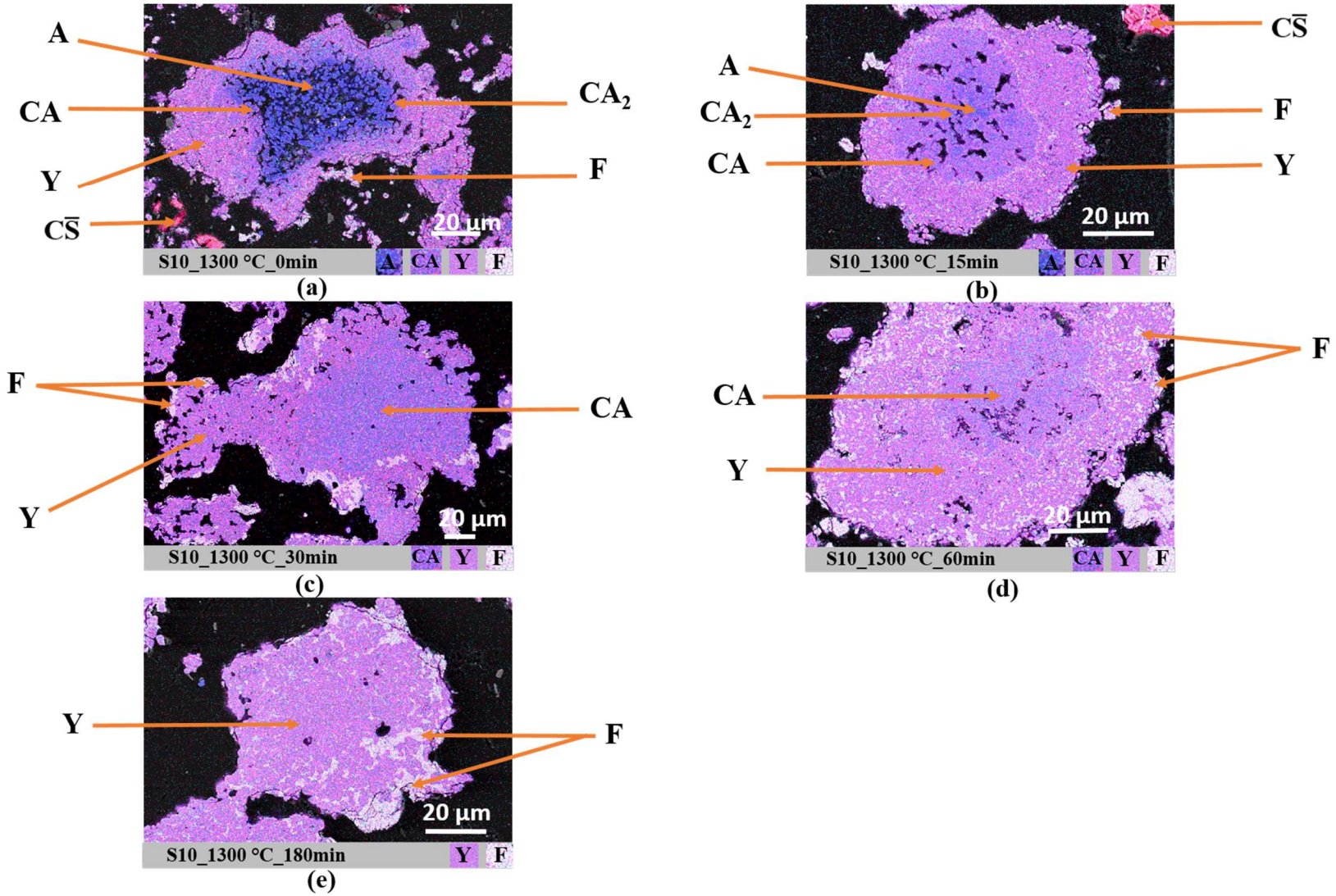

Fig. 9. EDS mapping of elements present in sample S10 treated at 1300 °C for different durations: 0 min (a), 15 min (b), 30 min (c), 60 min (d), and 180 min (e). Symbols: Y=Ye'elimite, CA_2=Grossite, CA=Krotite, F=Ferritic phase, A=Alumina, $C\overline{S}$=Calcium sulfate.

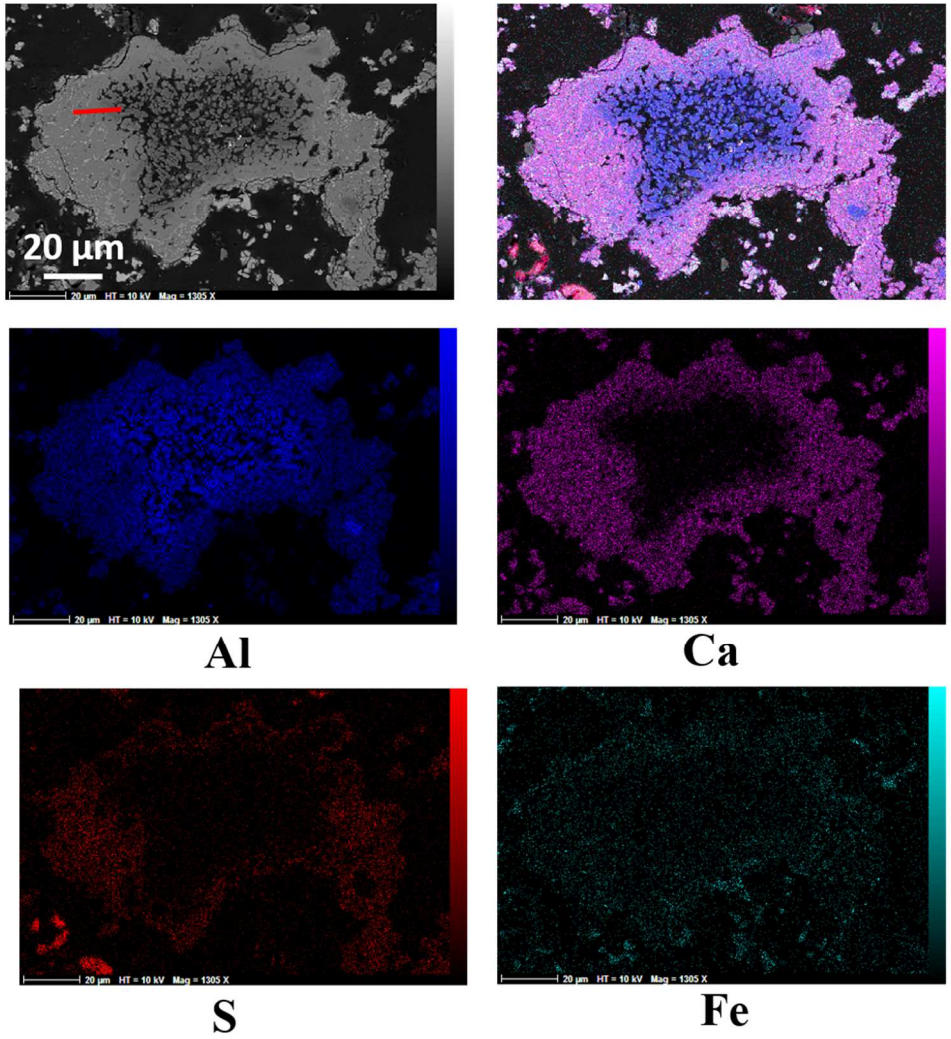
20 µm
Al
Ca
S
Fe

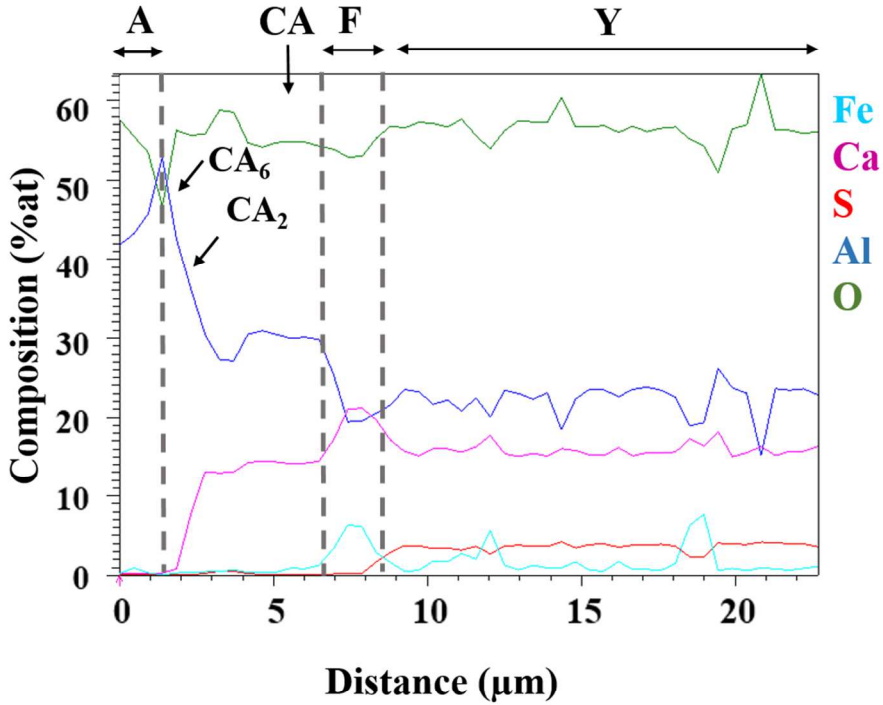
A
CA
F
Y
CA6
CA2
Composition (%at)
Distance (µm)
Fe
Ca
S
Al
O

Fig. 10–a

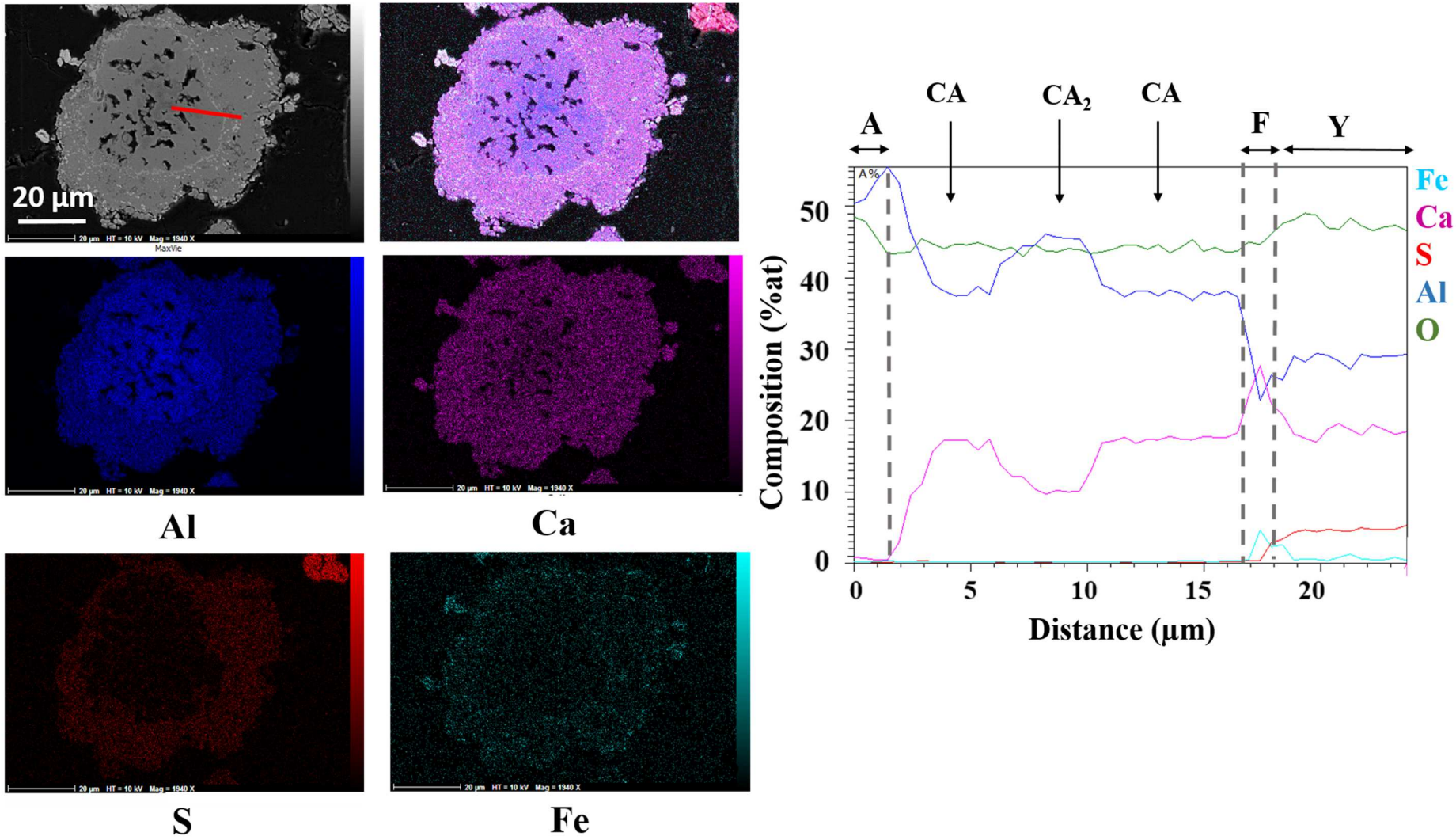
20 µm
Al
Ca
S
Fe
A
CA
CA2
CA
F
Y
A%
Fe
Ca
S
Al
O
Composition (%at)
Distance (µm)
0
10
20
30
40
50
0
5
10
15
20

Fig. 10–b

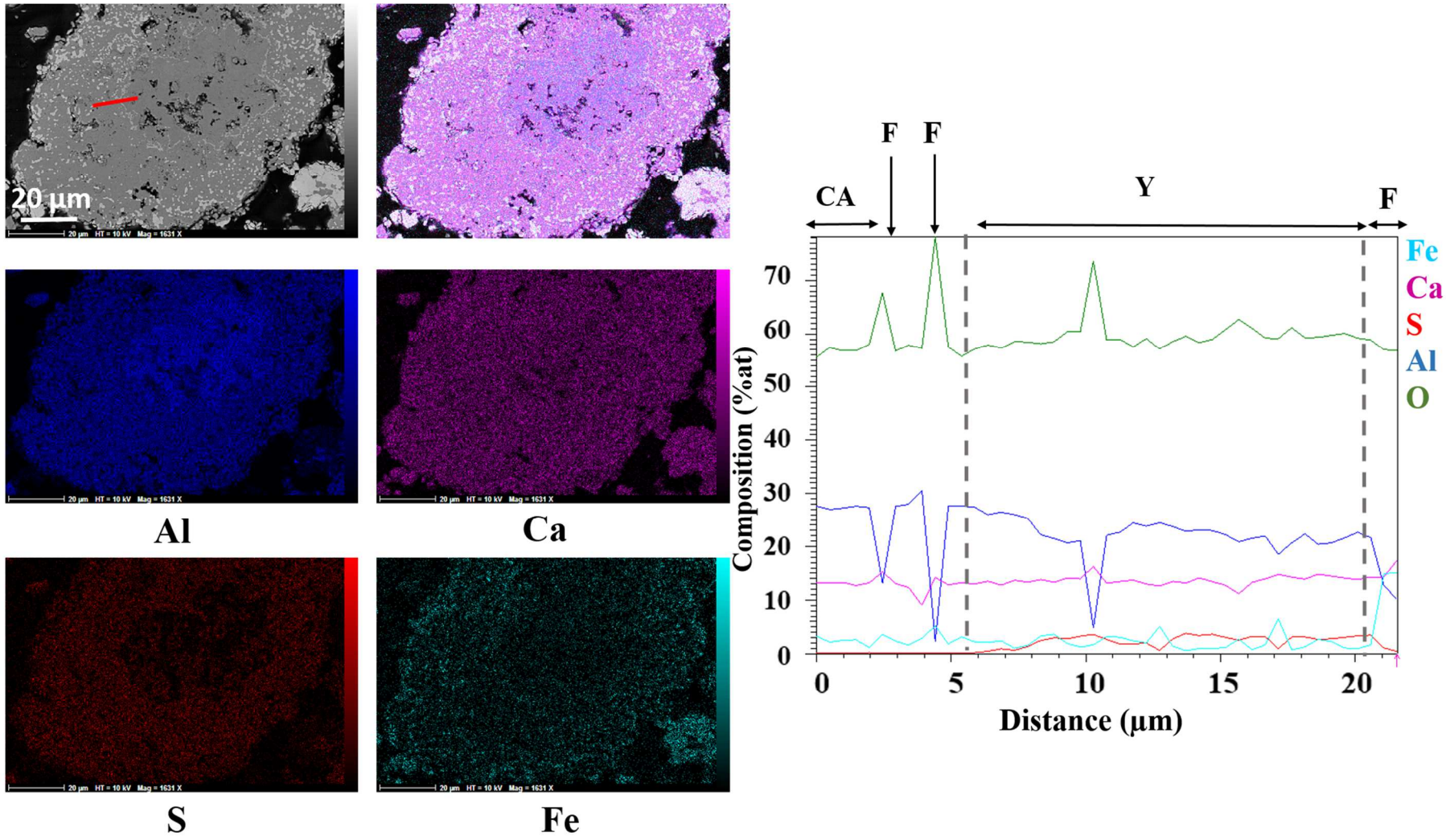
20 µm
Al
Ca
S
Fe
F
F
CA
Y
F
Fe
Ca
S
Al
O
Composition (%at)
0
10
20
30
40
50
60
70
0
5
10
15
20
Distance (µm)

Fig. 10–c

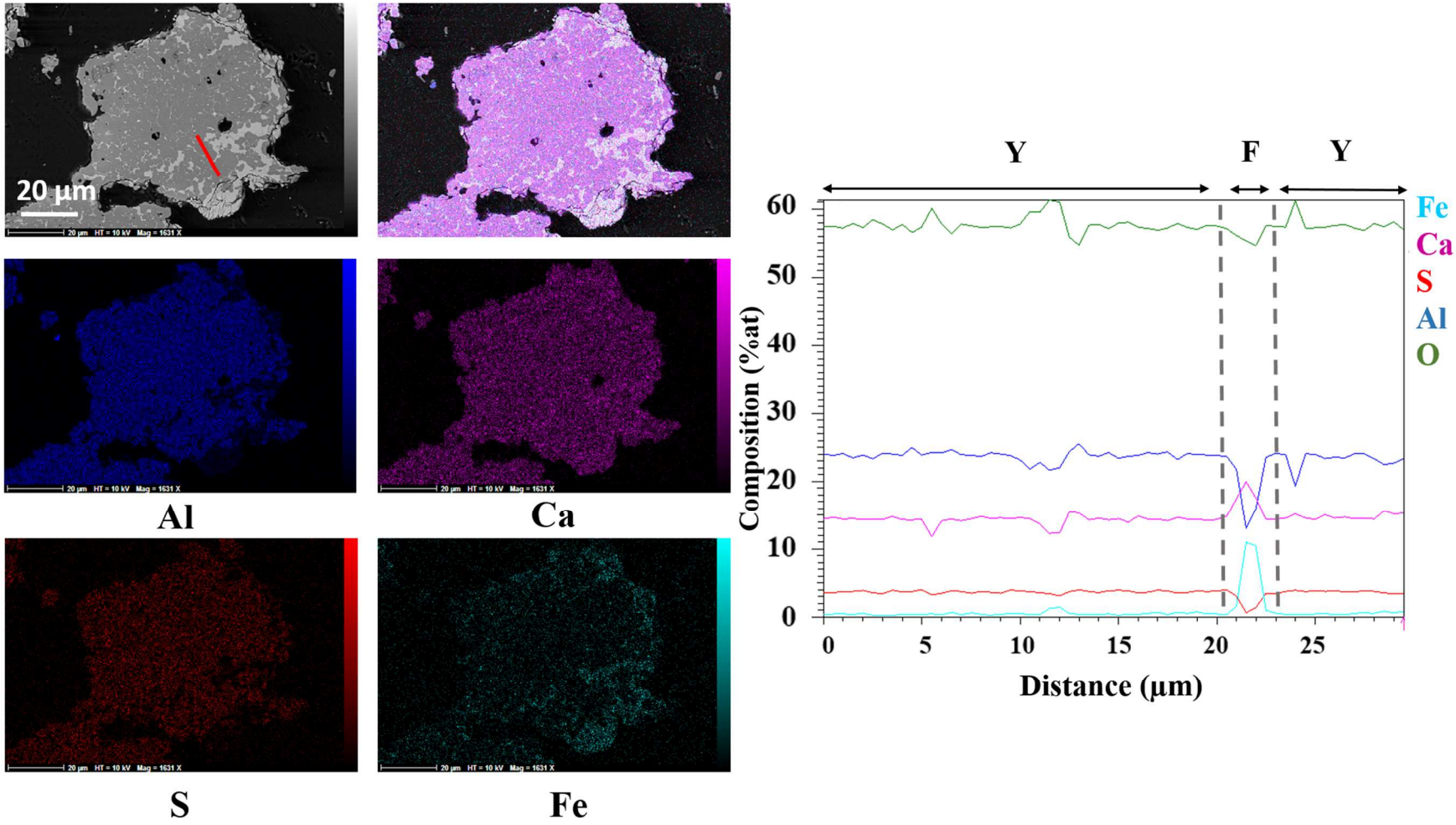

Fig. 10–d

Fig. 10. EDS mapping presenting the distribution of all elements and composition profiles obtained by EDS analysis, presenting the atomic percentages of the elements Ca, Al, S, Fe and O as a function of the location along the red lines drawn on the micrographs of the sample S10 treated at 1300 °C for different durations: 0 min (a), 15 min (b), 60 min (c), and 180 min (d).

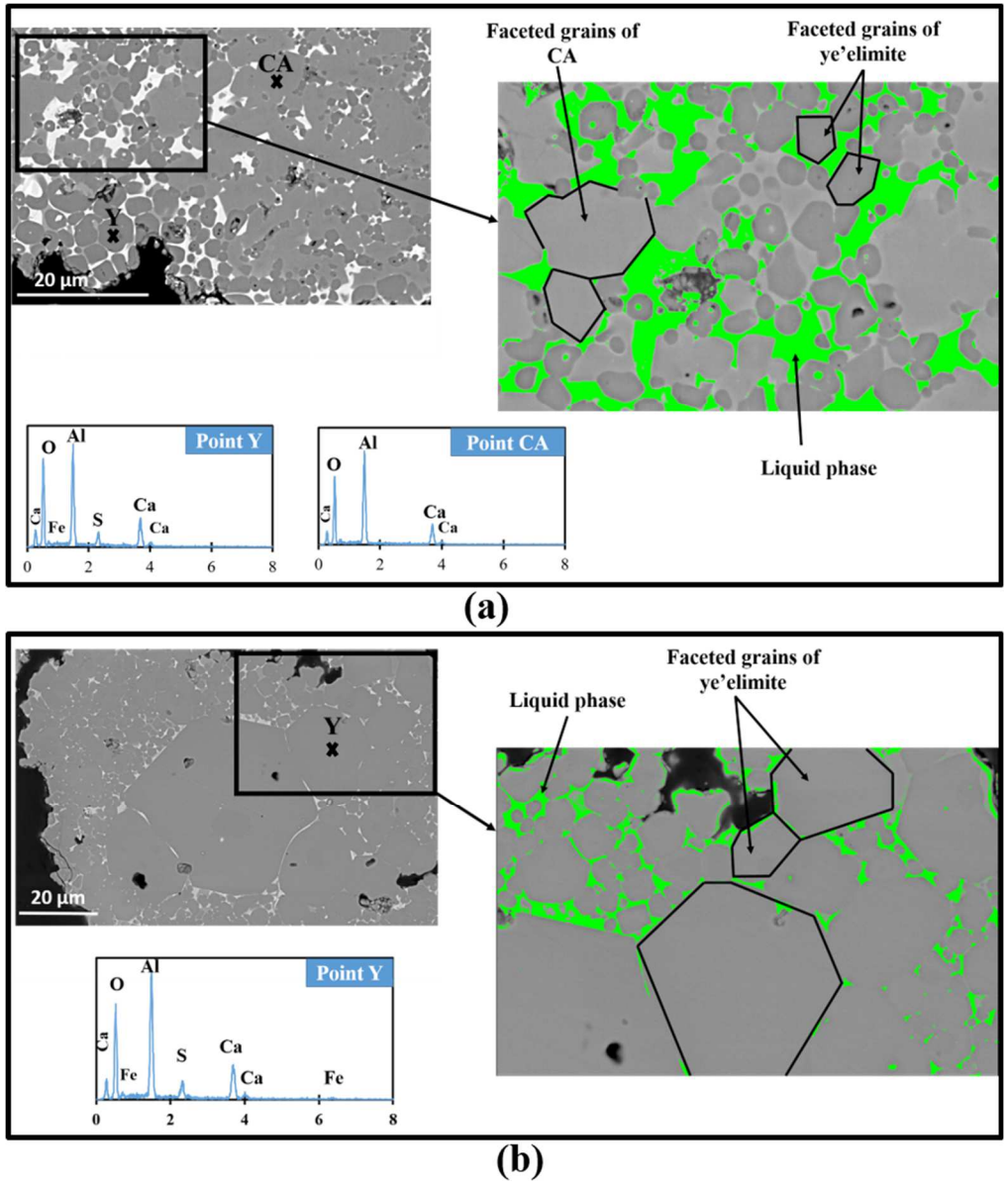

Fig. 11. SEM micrographs of the S10 sample sintered at 1300 °C for 60 min (a) and 180 min (b). The zooms show the distinction between the faceted grains of ye'elimite and CA resulting from liquid phase sintering. The corresponding EDS point analyses for each phase are shown.

		CA grain size distribution	Ye'elimite grain size distribution
S10_1300 °C_30min	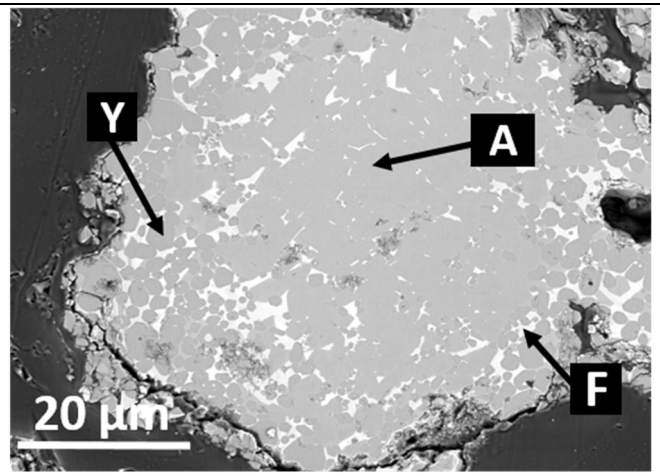	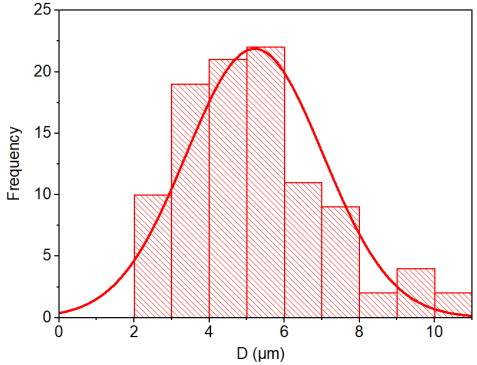 N_{total} = 100; Mean size = 5.20 µm; Standard Deviation = 1.82 µm	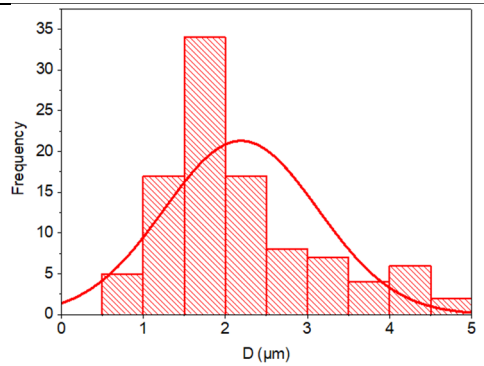 N_{total} = 100; Mean size = 2.19 µm; Standard Deviation = 0.93 µm
S10_1300 °C_60min	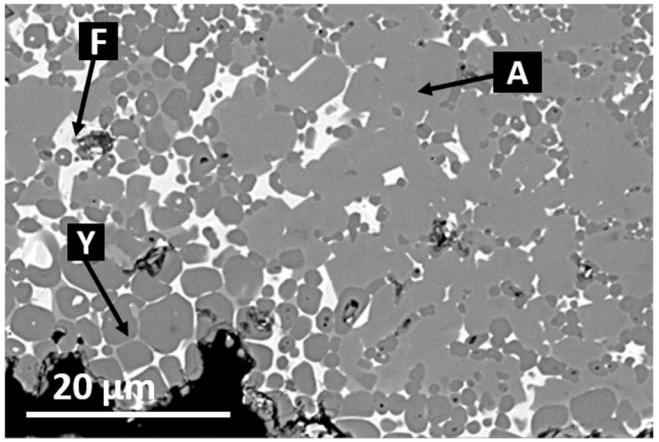	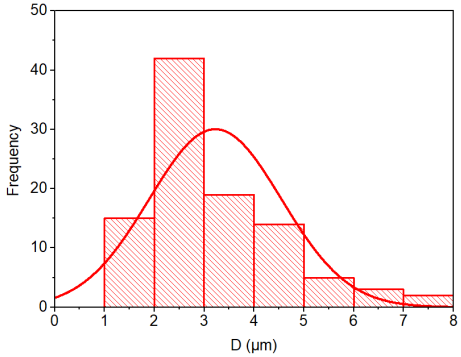 N_{total} = 100; Mean size = 3.22 µm; Standard Deviation = 1.32 µm	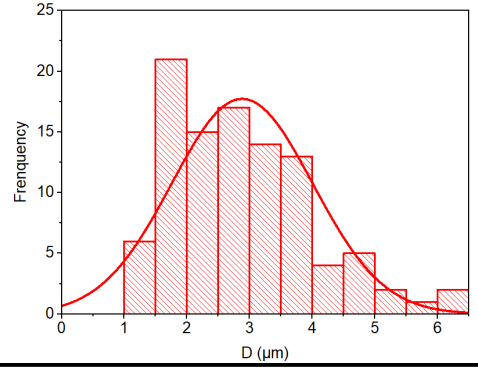 N_{total} = 100; Mean size = 2.88 µm; Standard Deviation = 1.12 µm
S10_1300 °C_180 min	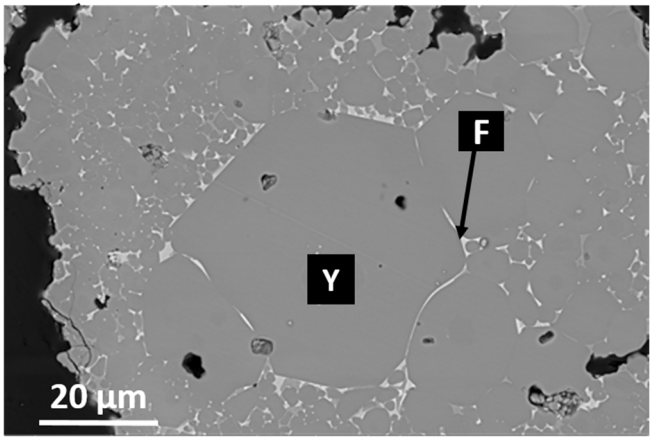		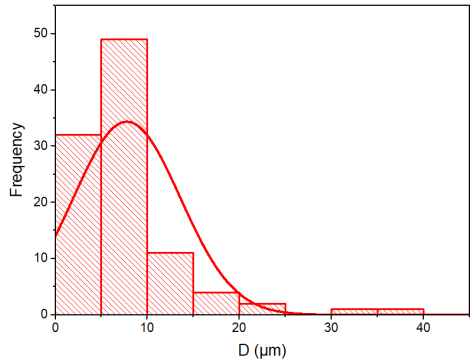 N_{total} = 100; Mean size = 7.76 µm; Standard Deviation = 5.80 µm

Fig.12. SEM micrographs of the S10 sample sintered at 1300 °C for 30 min, 60 min and 180min.

The particle size distribution of CA and ye'elimite grains was examined by PSD-IA from a total of 100 particles to determine the average diameter and deviation.

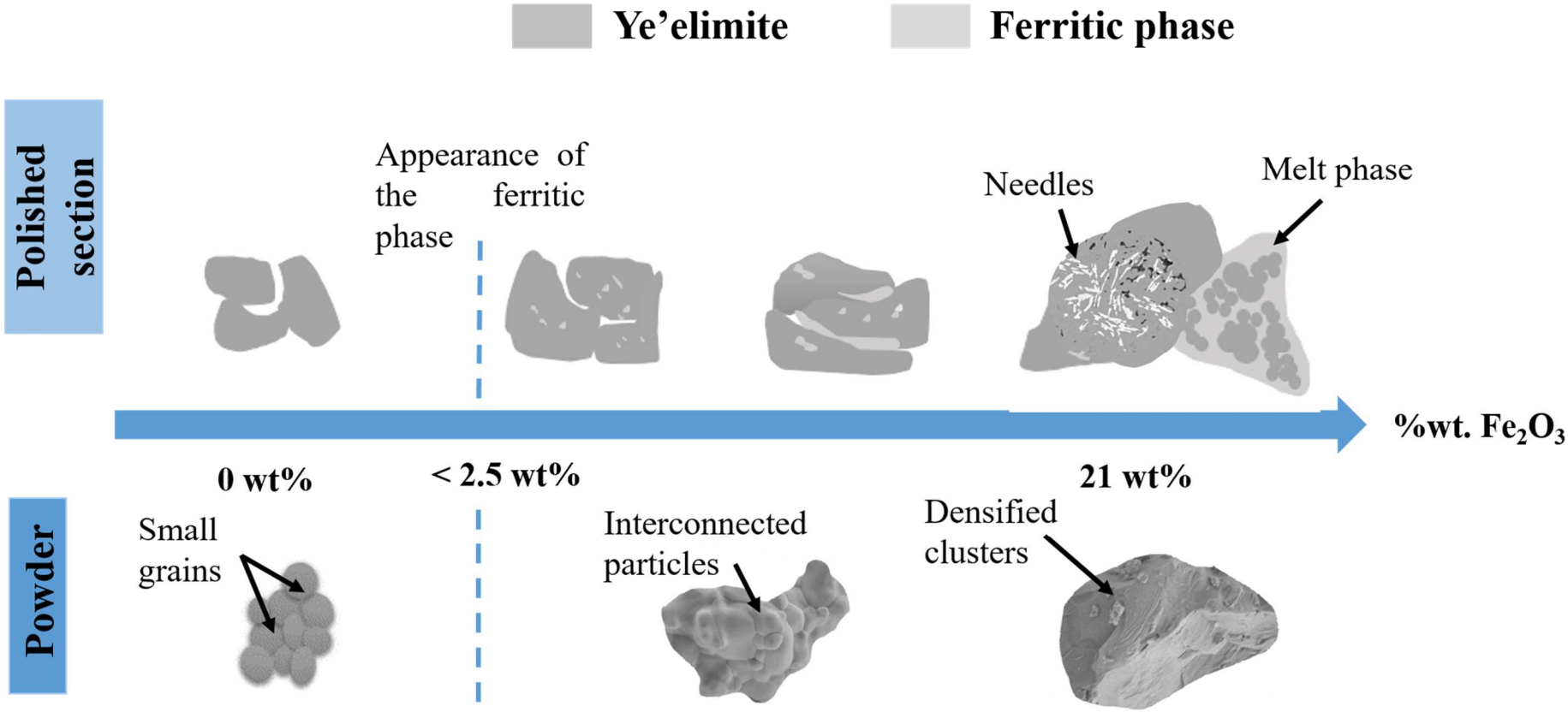
Ye'elimite
Ferritic phase
Polished section
Appearance of the ferritic phase
Needles
Melt phase
%wt. Fe_2O_3
0 wt%
< 2.5 wt%
21 wt%
Powder
Small grains
Interconnected particles
Densified clusters

Fig. 13–a

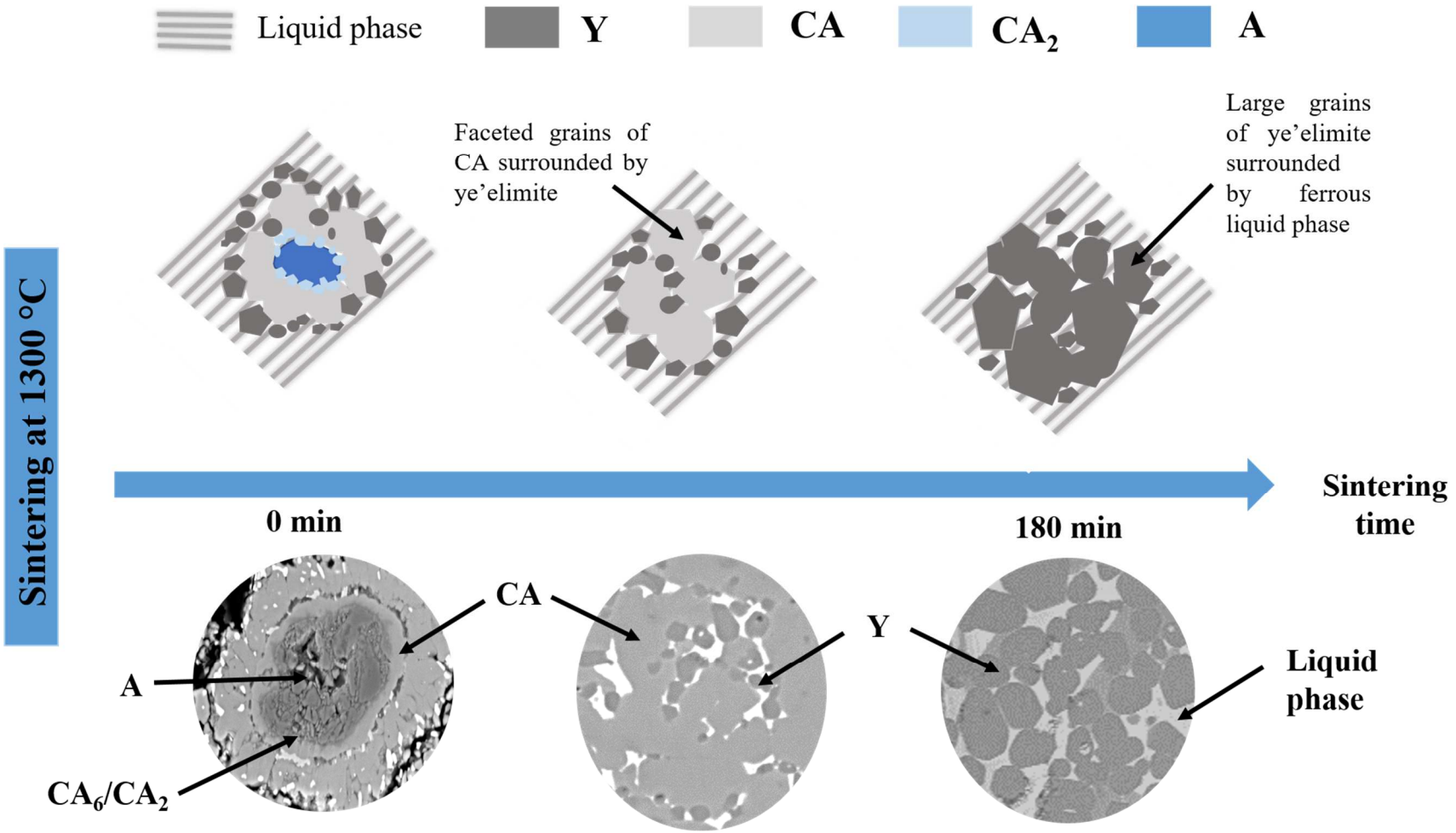

Fig. 13–b

Fig. 13. Schematic representation of microstructural development of the phases according to the percentage of Fe_2O_3 (a) and of the microstructural development of the phases in the presence of iron, according to the sintering time at 1300 °C (b).

Table 1

Summary of synthesis conditions described in previous works for solid-state synthesis of ye'elimite. (*) x represents the number of moles of substitution of Al_2O_3 by Fe_2O_3.

Solid-solution ye'elimite formula	Studied samples	Synthesis conditions					The maximum substitution level	Secondary phases	Ye'elimite polymorph	References
		Raw materials	Amount of raw material mixture (g)	Synthesis temperature (°C)	Sintering duration (hours)	heating rate (°C/min)				
$C_4A_{3-x}F_x\overline{S}$	$0 \leq x^{(*)} \leq 3$	$CaCO_3$, Al_2O_3, Fe_2O_3 and $CaSO_4.2H_2O$	20	1250	-	-	21.5 wt% Fe in $C_4A_3\overline{S}$ phase ($x^{(*)} \sim 1.5$)	$C\overline{S}$, CA, C_2F	Orthorhombic	M. Idrissi et al. [3]
$C_4A_{3-x}F_x\overline{S}$	x = 0.00, 0.05, 0.08, 0.20, 0.40 and 0.80	$CaCO_3$, Al_2O_3, Fe_2O_3 and $CaSO_4.2H_2O$	-	1250 - 1300	1	-	$x \sim 0.27$	$C_{12}A_7$, CA, CA_2, C_4AF, F, $C\overline{S}$, M and MA	Orthorhombic and cubic	F. Bullerjanh et al. [9]
$C_4A_{3-x}F_x\overline{S}$	$0 \leq x \leq 2$	$CaCO_3$, Al_2O_3, Fe_2O_3 and $CaSO_4.2H_2O$	-	1000 then 1325	1	-	$x \sim 0.34$	Ferrite, liquid phase	Cubic	B. Touzo et al. [16]
$C_4A_{2.8}F_{0.2}\overline{S}$	$x \sim 0.2$	-	-	1250	2	-	-	$C_{12}A_7$, CA, F and $C\overline{S}$	Cubic with traces of orthorhombic	F. Bullerjanh et al. [10]
$3CaCO_3$ - (3-x)Al_2O_3 - xFe_2O_3 - $CaSO_4$ - $2H_2O$	x = 0, 0.2, 0.4, 0.6, 0.8, 1.0, 1.2 and 1.4	$CaCO_3$, Al_2O_3, Fe_2O_3 and $CaSO_4.2H_2O$	-	1350	3	-	22.61 wt% Fe_2O_3 ($x \sim 1.2$)	$C_2(A,F)$, CA and C_3A	Cubic	D. Chen et al. [11]
$Ca_{3.8}Na_{0.2}Al_{5.6}Fe_{0.2}Si_{0.2}O_{12}SO_4$	-	$CaCO_3$, Al_2O_3, Fe_2O_3, SiO_2, Na_2CO_3 and $CaSO_4.2H_2O$	8	1250	4	5	-		Cubic	A. Cuesta et al. [12]
$Ca_{4.25}Si_{0.02}Al_{5.96}Fe_{0.16}S_{0.85}O_{16}$	The six clinkers	$CaCO_3$, Al_2O_3, Fe_2O_3, $CaSO_4.2H_2O$	-	1000 then 1000	1 0.5	-	$x \sim 0.08$	Clinker phases: small	-	J. Strigac et al. [13]

		and silica gel		then 1450	0.25			amount of free lime, β-C_2S, $C_4A_3\overline{S}$, C_4AF and $C\overline{S}$		
$C_4A_{3-x}F_x\overline{S}$	x = 0.16, 0.21, 0.25, 0.32	$CaCO_3$, Al_2O_3, Fe_2O_3, $CaSO_4$	-	1300	22	-	x ~ 0.32	Ferritic phase	-	N. Zupancic et al. [14]
$Ca_4(Al_{1-x}Fe_x)_6SO_{16}$	x = 0.00, 0.02, 0.05, 0.07, 0.1, 0.12, 0.15 and 0.25	$CaCO_3$, $Al(OH)_3$, $CaSO_4.2H_2O$ and Fe_2O_3	5	50 - 800 then 800 – 1000 then 1000 - 1250	- - 5	5 3 2	10 wt% Fe_2O_3 in basic materials (x ~ 0.3)	CA, $C_{12}A_7$ and C_2F	Orthorhombic and cubic	J.S. Ndzila et al. [15]

Table 2

Amounts (wt. %) of the raw materials to prepare S0-S21 samples.

Sample name	%Fe_2O_3	%$CaCO_3$	%Al_2O_3	%$CaSO_4.2H_2O$	x
S0	0.00	38.57	39.31	22.12	0
S1	1.01	38.43	38.52	22.04	0.05
S2	2.01	38.30	37.74	21.96	0.1
S2.5	2.53	38.22	37.33	21.92	0.12
S5	5.11	37.86	35.32	21.71	0.25
S10	10.44	37.12	31.15	21.29	0.53
S21	21.38	35.60	22.61	20.41	1.13

Table 3

Polishing protocol for samples prepared in resin.

Step	SiC abrasive paper	Time (s)	Rotation speed of the polishing disc (rpm)
1	P120	30	150
2	P240	from 50 to 60	150
3	P600	180	150
4	P1200	270	150
5	P2400	420	150
6	P4000	600	150

Table 4

ICSD collection codes for phases used in the Rietveld analysis quantification.

	Cementitious notation	Chemical formula in ICSD file	ICSD Codes	Ref.
Orthorhombic ye'elimite	orth-$C_4A_3\overline{S}$	$Ca_4Al_6SO_{16}$	80361	[28]
Cubic ye'elimite	cub-$C_4A_3\overline{S}$	$Ca_4Al_6(SO_4)O_{12}$	9560	[29]
Krotite	CA	$CaAl_2O_4$	260	[30]
Grossite	CA_2	$CaAl_4O_7$	34487	[31]
Ferritic phase	C_2(A,F)	$Ca_2Fe_{1.28}Al_{0.72}O_5$	2842	[19]
Calcium sulfate	$C\overline{S}$	$Ca(SO_4)$	16382	[32]
Lime	C	CaO	52783	[33]
Alumina	A	Al_2O_3	73725	[34]

Table 5

Quantitative Rietveld analysis of phases in samples S0, S1, S2.5, S5, S10 and S21 heat-treated at 1300 °C. The values in brackets correspond to the error by the quantitative Rietveld analysis. (*) Rwp is the weighted profile factor and Rexp is the expected factor.

	S0	S1	S2.5	S5	S10	S21
orth-$C_4A_3\overline{S}$ (wt. %)	83.1 (±0.7)	89.3 (±2)	75.8 (±2)	73.2 (±2)	62.0 (±2)	28.6 (±2)
cub-$C_4A_3\overline{S}$ (wt. %)	-	9.4 (±2)	22.6 (±2)	25.4 (±2)	30.1 (±2)	56.7 (±2)
CA (wt. %)	7.8 (±0.7)	0.6 (±0.1)	0.6 (±0.1)	0.7 (±0.1)	1.2 (±0.2)	3.3 (±0.4)
CA_2 (wt. %)	9.1 (±0.4)	0.7 (±0.1)	0.8 (±0.1)	-	-	-
C_2(A,F) (wt. %)	-	-	0.2 (±0.1)	0.7 (±0.1)	6.7 (±0.5)	11.4 (±0.8)
R_{WP} (*)	12.3	8.5	9.5	12.0	14.2	27.5
Rexp (*)	4.4	4.6	4.9	4.8	5.0	8.1